Article

Cell

Enterochromaffin Cells Are Gut Chemosensors that Couple to Sensory Neural Pathways

Graphical Abstract

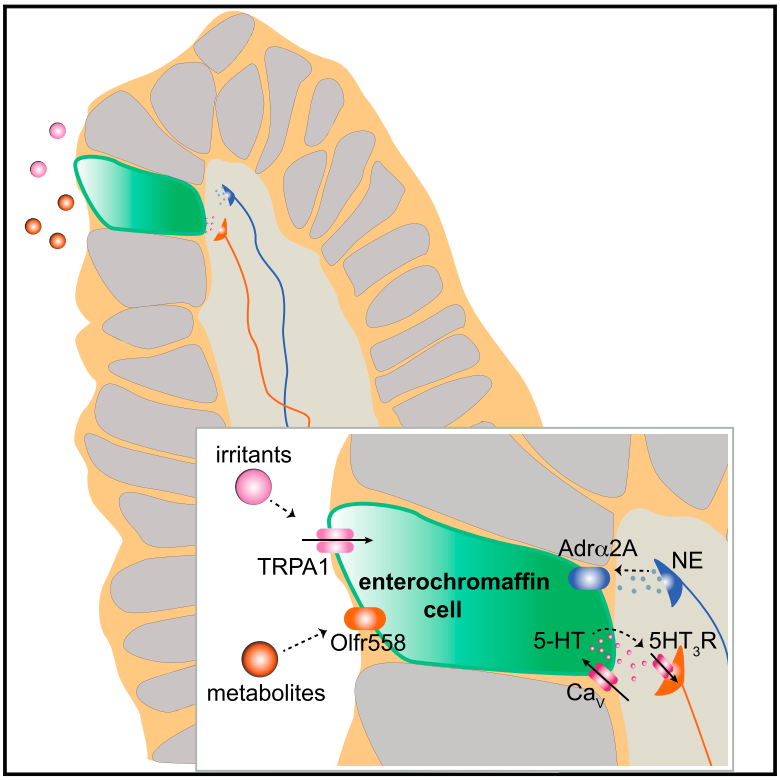

Authors

Nicholas W. Bellono, James R. Bayrer, Duncan B. Leitch, ..., Stuart M. Brierley, Holly A. Ingraham, David Julius

Correspondence

holly.ingraham@ucsf.edu (H.A.I.), david.julius@ucsf.edu (D.J.)

In Brief

Organoid cultures are exploited to characterize rare chemosensory cells in the gut, revealing their receptive and signaling properties and demonstrating direct communication with neural sensory pathways.

Highlights

- Enterochromaffin (EC) cells are excitable and express voltage-gated ion channels
- EC cells use sensory receptors to detect irritants, metabolites, and catecholamines
- EC cell activation leads to voltage-gated Ca^{2+} channel-dependent serotonin release
- EC cells modulate sensory nerves via serotonin receptors and synaptic connections

Bellono et al., 2017, Cell *170*, 1–14
June 29, 2017
http://dx.doi.org/10.1016/j.cell.2017.05.034

CellPress

Please cite this article in press as: Bellono et al., Enterochromaffin Cells Are Gut Chemosensors that Couple to Sensory Neural Pathways, Cell (2017), http://dx.doi.org/10.1016/j.cell.2017.05.034

Cell

Enterochromaffin Cells Are Gut Chemosensors that Couple to Sensory Neural Pathways

Nicholas W. Bellono,[1,6] James R. Bayrer,[2,3,6] Duncan B. Leitch,[1] Joel Castro,[4,5] Chuchu Zhang,[1] Tracey A. O'Donnell,[4,5] Stuart M. Brierley,[4,5] Holly A. Ingraham,[3,*] and David Julius[1,7,*]

[1]Department of Physiology, University of California, San Francisco, San Francisco, CA 94143, USA
[2]Department of Pediatrics, Division of Gastroenterology, University of California, San Francisco, San Francisco, CA 94143, USA
[3]Department of Cellular and Molecular Pharmacology, University of California, San Francisco, San Francisco, CA 94143, USA
[4]Visceral Pain Group, Flinders University, Bedford Park, SA 5042, Australia
[5]Centre for Nutrition and Gastrointestinal Diseases, Discipline of Medicine, University of Adelaide, South Australian Health and Medical Research Institute (SAHMRI), North Terrace, Adelaide, SA 5000, Australia
[6]These authors contributed equally
[7]Lead Contact
*Correspondence: holly.ingraham@ucsf.edu (H.A.I.), david.julius@ucsf.edu (D.J.)
http://dx.doi.org/10.1016/j.cell.2017.05.034

SUMMARY

Dietary, microbial, and inflammatory factors modulate the gut-brain axis and influence physiological processes ranging from metabolism to cognition. The gut epithelium is a principal site for detecting such agents, but precisely how it communicates with neural elements is poorly understood. Serotonergic enterochromaffin (EC) cells are proposed to fulfill this role by acting as chemosensors, but understanding how these rare and unique cell types transduce chemosensory information to the nervous system has been hampered by their paucity and inaccessibility to single-cell measurements. Here, we circumvent this limitation by exploiting cultured intestinal organoids together with single-cell measurements to elucidate intrinsic biophysical, pharmacological, and genetic properties of EC cells. We show that EC cells express specific chemosensory receptors, are electrically excitable, and modulate serotonin-sensitive primary afferent nerve fibers via synaptic connections, enabling them to detect and transduce environmental, metabolic, and homeostatic information from the gut directly to the nervous system.

INTRODUCTION

The gut epithelium forms one of the largest exposed surfaces of the human body, representing a unique interface for integrating environmental information with physiologic signals from nervous, immune, and vascular systems (Furness et al., 2013; Öhman et al., 2015). Dietary nutrients and irritants, microbiota products, and inflammatory agents have been proposed to act on the gut epithelium to modulate downstream signaling pathways controlling digestion, immunity, metabolism, and pain (Brierley and Linden, 2014; Furness et al., 2013). Diverse enteroendocrine cells within the gut epithelium respond to such stimuli by releasing a variety of hormones to mediate physiologic responses (Gribble and Reimann, 2016). Indeed, enteroendocrine cells form anatomical connections with neurons (Bohórquez et al., 2015), consistent with the idea that the epithelium participates in neural monitoring of the gut environment. Despite growing interest in the gut-neural axis, relatively little is known about molecular mechanisms underlying chemosensory transduction by the gut epithelium, or how this information is transmitted to the nervous system.

The enterochromaffin (EC) cell is an enteroendocrine cell subtype that represents one of the major proposed epithelial chemosensors. Although relatively rare (<1% of total intestinal epithelia), these unique cells produce >90% of the body's serotonin and have been suggested to affect a variety of physiological and pathophysiological states, such as gastrointestinal (GI) motility and secretion, nausea, and visceral hypersensitivity (Gershon, 2013; Mawe and Hoffman, 2013). Previous studies suggest that EC cells express sensory receptors whose activation promotes release of 5-HT with consequent stimulation of gut contractility. While informative, these initial insights have generally been gleaned from model endocrine tumor cell lines or ex vivo whole tissue preparations (Braun et al., 2007; Doihara et al., 2009; Fukumoto et al., 2003; Hagbom et al., 2011; Kim et al., 2001; Nozawa et al., 2009), leaving fundamental questions unanswered. For example, what stimuli or downstream signaling pathways promote serotonin release from EC cells, and how do EC cells communicate with the nervous system?

To address such questions it is necessary to directly interrogate single EC cells, but this is technically challenging given their relatively small size (<10 μm) and paucity. We therefore generated intestinal organoids in which EC cells are genetically tagged to facilitate their detailed physiologic, pharmacologic, and molecular characterization in a "native" environment. We show that EC cells are electrically excitable because they express functional voltage-gated sodium (Na^+) and calcium (Ca^{2+}) channels, akin to other primary sensory cells. Moreover, EC cells use specific receptors and signal transduction pathways to detect relevant stimuli: the transient receptor potential A1 (TRPA1) ion channel serves as an irritant receptor, olfactory receptor 558 (Olfr558) serves as a microbial metabolite sensor,

and an α2A adrendoreceptor (Adrα2A)-TRPC4 channel signaling cascade detects stress response-related catecholamines. These sensory transduction pathways stimulate P/Q-type voltage-gated Ca^{2+} channels to control serotonin release onto $5HT_3$ receptor-expressing primary afferent nerve fibers that extend into intestinal villi and engage in synaptic-like contacts with EC cells. Our findings establish EC cells as specialized, polymodal stimulus detectors that constitute a direct line of communication between the gut epithelium and specific primary afferent nerve fibers. This signaling system represents a key pathway for monitoring GI commensal or infectious microbes, injury, or other changes to the luminal environment that stimulate physiologic responses such as emesis, motility, and visceral pain.

RESULTS

EC Cells Are Electrically Excitable

We used mice expressing a genetically encoded fluorescent protein (hrGFP) under control of the *chromogranin A* (*ChgA*) promoter to selectively label EC cells for single-cell characterization (Figure 1A). Consistent with previous results (Engelstoft et al., 2015), we found that ChgA-GFP co-localized with serotonin, but not with lysozyme or GLP-1, which mark Paneth or peptide hormone-producing enteroendocrine cells, respectively (Figures 1A and S1A–S1C). Furthermore, transcriptional profiling of ChgA-GFP^+ cells revealed enrichment of EC cell markers but not markers for hormone-producing enteroendocrine cells (Figure S1D). We used whole-cell patch-clamp recording to analyze the electrophysiological properties of single EC cells from native intestinal tissue or intestinal organoids derived from these animals (Figures 1B and 1C). We first observed a large outward current in response to voltage ramps that was blocked by tetraethylammonium (TEA^+) (Figure 1B), indicating that the current is carried by K^+ channels, several subtypes of which were expressed at high levels in EC cells (Figure S2A). Acute TEA^+ treatment revealed small voltage-activated inward currents that we further characterized in the presence of intracellular Cs^+ to block K^+ channels (Figure 1B). Under these conditions, voltage-steps elicited rapidly-inactivating tetrodotoxin-sensitive inward currents in EC cells from intestinal organoids or native intestine, suggesting the presence of voltage-gated sodium (Na_V) channels (Figures 1C and 1D). Steady-state activation and inactivation properties of this current were consistent with properties of the $Na_V1.3$ subtype of voltage-gated Na^+ channels (Catterall et al., 2005a), whose transcripts were highly enriched in EC cells (Figures 1E and S2B). Furthermore, we found that EC cells are electrically excitable, producing tetrodotoxin-sensitive action potentials (Figure 1F).

In addition to the transient Na_V current, we observed a small voltage-activated slowly-inactivating current (Figure S2C). We reasoned that voltage-gated Ca^{2+} channels (Ca_V) might contribute to this current because of its slow inactivation kinetics and the fact that Ca_V channels have been previously implicated in EC cell function (Racké and Schwörer, 1993; Raghupathi et al., 2013). Indeed, when intestinal epithelial cells were depolarized with high extracellular K^+, we observed large increases in intracellular Ca^{2+} predominantly within EC cells (Figures 1G and 1H). Moreover, depolarization-evoked Ca^{2+} responses were inhibited by ω-agatoxin IVA, which blocks presynaptic P/Q-type Ca_V channels (Catterall et al., 2005b) (Figures 1H and 1I). A subset of EC cells were basally active, exhibiting spontaneous Ca^{2+} bursts that were attenuated by tetrodotoxin or blocked by ω-agatoxin IVA (Figure S2D). Consistent with this pharmacological profile, P/Q-type $Ca_V2.1$ channel transcripts were selectively expressed in EC cells (Figure 1J). Transcripts for the low voltage threshold T-type channel, $Ca_V3.2$, were also highly enriched in EC cells. Perhaps not surprisingly, a T-type Ca_V channel inhibitor did not significantly affect K^+-induced responses (Figure 1I), consistent with the fact that $Ca_V3.2$ often functions in amplifying signals from low threshold stimuli or regulating membrane potential (Catterall et al., 2005b). In summary, our results show that EC cells express voltage-gated ion channels, rendering them electrically excitable—a hallmark of sensory cell types. Indeed, our findings with serotonergic EC cells are similar to what has been observed with hormone-secreting L-type enteroendocrine cells, which also express Nav and Cav channels that render them electrically excitable (Rogers et al., 2011).

EC Cells Are Polymodal Chemosensors

To ask if EC cells serve a specific chemosensory role, we screened 30 potential agonists, focusing on compounds known to be present in the gut, including microbial products, irritants and inflammatory agents, and neurotransmitters. Among these, only allyl isothiocyanate (AITC), isovalerate, and the catecholamines dopamine, epinephrine, or norepinephrine specifically and consistently activated EC cells (Figure 2A). Additionally, isobutyrate and butyrate elicited small, but consistent responses (Figure 2A). Each of these compounds evoked Ca^{2+} transients, or in some cases oscillatory responses resembling the Na_V- and Ca_V-dependent bursting activity that we observed in subsets of EC cells (Figure S2D). Remarkably, this activity profile is directly relevant to the etiology of GI inflammation. For instance, AITC, the pungent agent in wasabi and other mustard plants, is representative of a class of reactive chemical irritants that elicit cutaneous and visceral inflammatory pain (Bautista et al., 2006; Brierley et al., 2009). Isovalerate, isobutyrate, and butyrate are volatile fatty acid fermentation products produced by gut microbiota that modulate serotonin biosynthesis (Yano et al., 2015) and are linked to several pathophysiological states (Koh et al., 2016). Lastly, homeostatic regulation of sympathetic signaling increases norepinephrine levels in the gut following infection, injury, and other types of GI stress (Gabanyi et al., 2016). Together, these results support the idea that EC cells serve as sentinels of noxious chemical stimuli or other insults affecting the GI tract.

Our EC cell transcriptional profile showed that sensory receptors are among the most enriched transcripts, with relative expression rivaling the EC cell marker tryptophan hydroxylase 1 (*Tph1*) or the pore-forming subunit of $Na_V1.3$ (*Scn3a*) (Figure 2B). Moreover, three of the most enriched sensory receptors are known to be involved in the detection of molecules identified in our screen. For example, transcripts encoding the AITC receptor, TRPA1, were enriched in EC cells (Figure 2B), consistent with previous histological analysis of intestinal tissue sections (Nozawa et al., 2009). Transcripts encoding

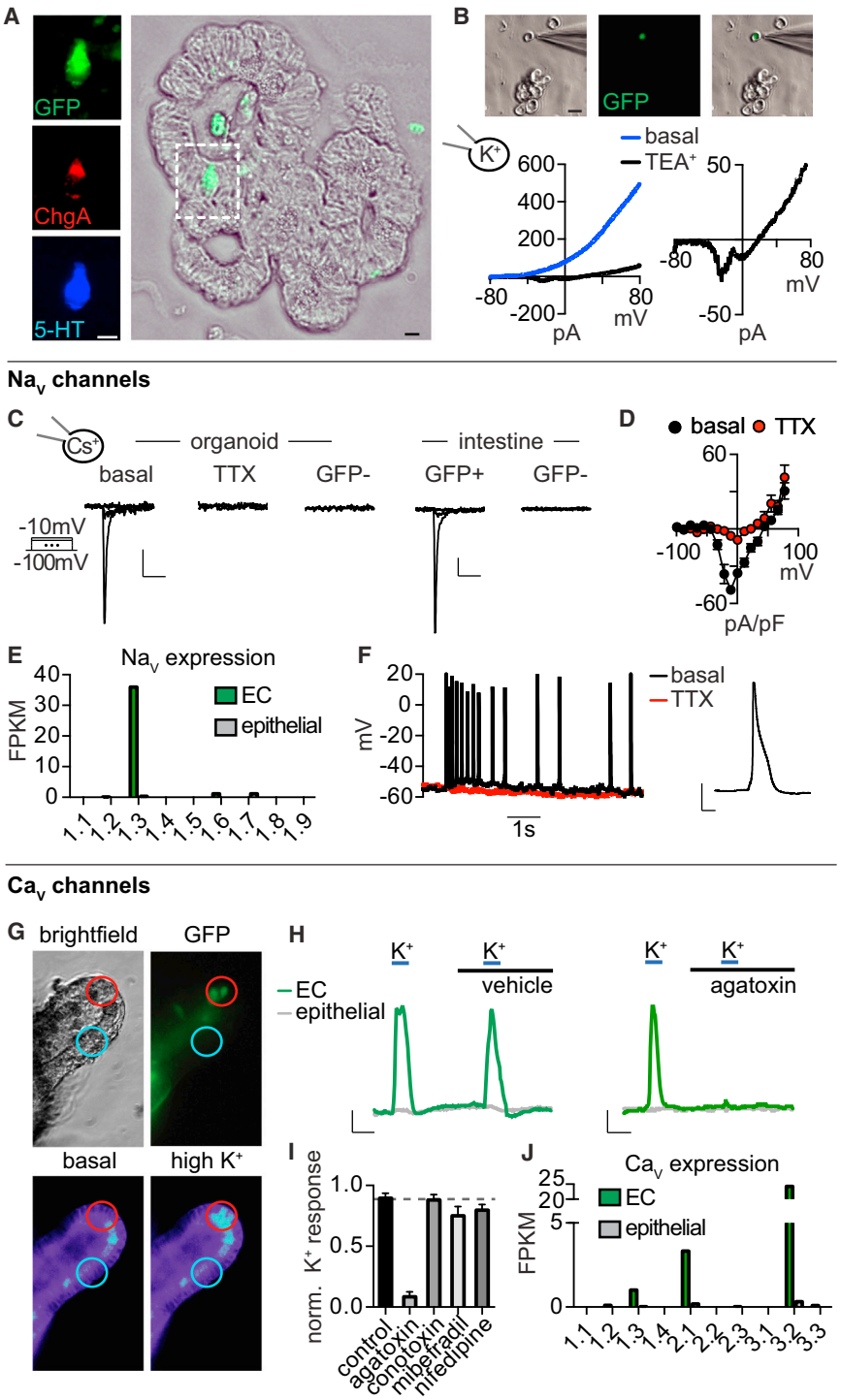

Figure 1. Enterochromaffin Cells Are Electrically Excitable

(A) Co-localization of chromogranin A-driven GFP reporter (ChgA-GFP, green), ChgA (red), and serotonin (5-HT, blue) labels enterochromaffin (EC) cells in intestinal organoids. Scale bar, 10 μm.

(B) Dissociated EC cell (green) in a representative patch-clamp experiment. Scale bar, 10 μm. In response to a voltage ramp, the representative K^+ current was blocked by 10 mM TEA^+ to reveal a voltage-activated inward current. Representative of n = 4 cells.

(C) Voltage-gated currents in EC cells were inhibited by the Na_V antagonist tetrodotoxin (TTX, 500 nM). Scale bars, 50 pA vertical, 10 ms horizontal.

(D) Average current-voltage relationship. n = 7. $p < 0.0001$ for basal versus TTX. Two-way ANOVA with post hoc Bonferroni test.

(E) mRNA expression profile of Na_V pore-forming subunits in EC cells (green) compared with other intestinal epithelial cells (gray). Bars represent fragments per kilobase of exon per million fragments mapped (FPKM).

(F) Spontaneous action potentials measured at resting membrane potential were inhibited by TTX. Representative of n = 4. Inset: representative action potential. Scale bar, 20 mV, 10 ms.

(G) Representative calcium (Ca^{2+}) imaging experiment from EC cells (GFP, green) in an intestinal organoid. High extracellular K^+ increased cytosolic Ca^{2+}, indicated by a change in fluorescence ratio of Fura-2AM.

(H) Ca^{2+} responses to K^+-elicited depolarization in EC (green) or neighboring cells (gray). The P/Q-type Ca_V inhibitor ω-agatoxin IVA abolished responses. Scale bar, 0.25 Fura-2 ratio, 50 s.

(I) Pharmacological profile of Ca_V-mediated responses. n = 6 per condition. Data represented as mean ± SEM. $p < 0.0001$ for control versus 300 nM ω-agatoxin IVA. One-way ANOVA with post hoc Bonferroni test. All data represented as mean ± SEM.

(J) mRNA expression profile of Ca_V pore-forming subunits in EC cells (green) compared with other intestinal epithelial cells (gray).

See also Figures S1 and S2.

olfactory receptors have been previously detected in EC cells (Braun et al., 2007), and our analysis similarly identified Olfr558 as a prevalent sensory receptor in these cells (Figure 2B). Indeed, orthologs of Olfr558 are widely expressed outside of the olfactory epithelium, including in endocrine cells of the GI tract, where expression is modulated by microbiota (Flegel et al., 2013; Priori et al., 2015). Consistent with our pharmacological screen, isovalerate has been identified as a putative agonist for Olfr558 (Audouze et al., 2014). Finally, the receptor-operated ion channel, TRPC4, is also preferentially expressed in EC cells (Figure 2B), where it functions as a key component of the catecholamine signal transduction pathway (see below). Transcripts encoding these sensory receptors and transducers were also expressed in EC cells from native intestine (Figure S3) (Nozawa et al., 2009). Thus, EC cells are polymodal chemosensors that are molecularly tuned to detect physiologically relevant stimuli.

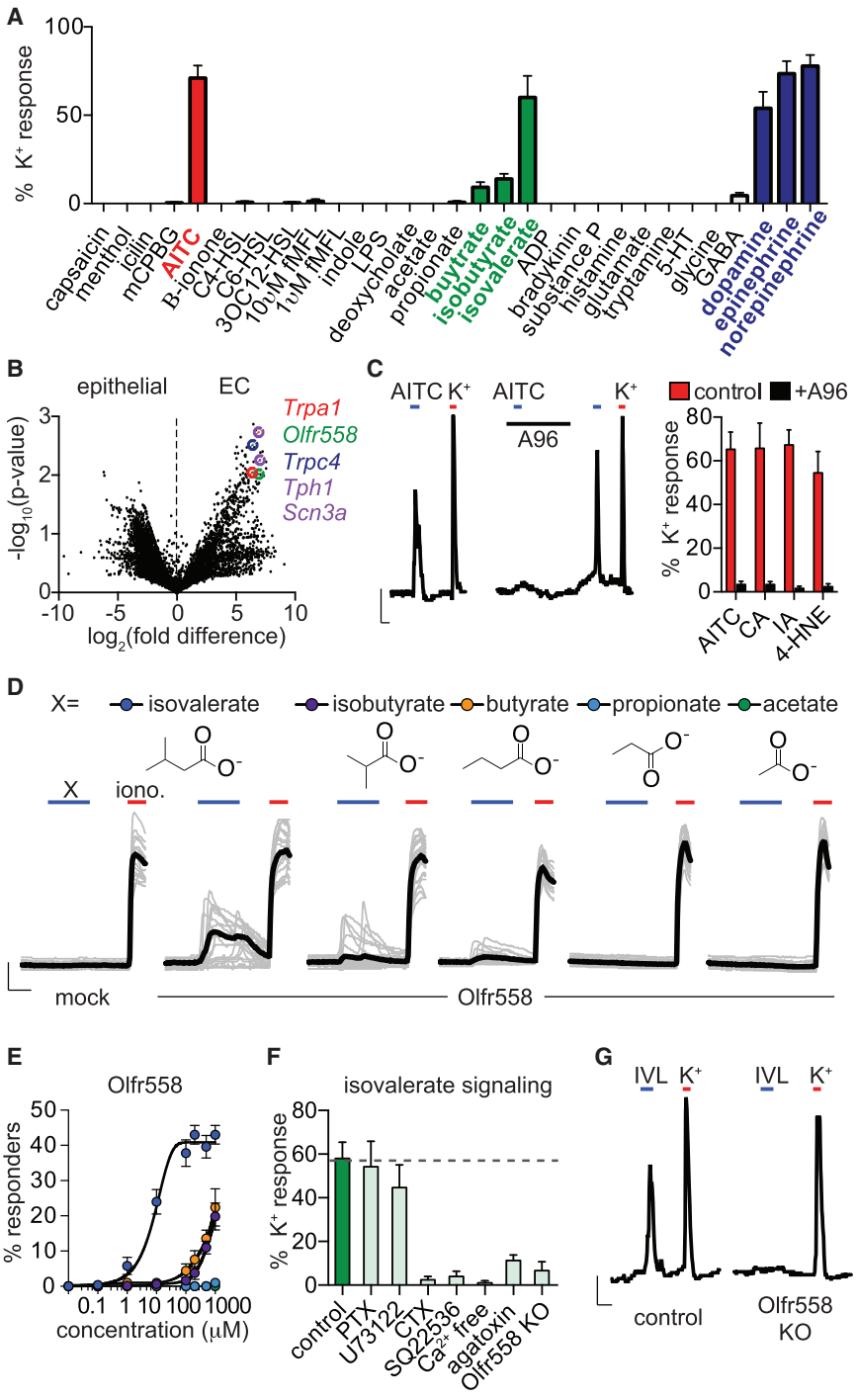

Figure 2. Enterochromaffin Cells Use TRPA1 as an Irritant Receptor and Olfr558 as a Metabolite Sensor

(A) Sensory molecule screen for EC cell-specific Ca^{2+} responses. High K^+ was added at the end of each experiment to induce maximal Ca^{2+} responses used for normalization. n = 6–62 per condition. Data represented as mean ± SEM.

(B) mRNA expression profile of EC cells compared with other intestinal epithelial cells shown as a volcano plot. *Trpa1* (red), *Olfr558* (green), and *Trpc4* (blue) were among the most enriched transcripts that encode sensory receptors or channels. EC cell marker *Tph1* and $Na_V1.3$ pore-forming subunit *Scn3a* are shown for comparison (purple).

(C) AITC (150 μM)-elicited Ca^{2+} responses were inhibited by the TRPA1 antagonist A967079 (A96, 10 μM). Scale bar, 0.1 Fura-2 ratio, 50 s. Average peak Ca^{2+} responses evoked by TRPA1 agonists AITC, cinnamaldehyde (CA, (150 μM), iodoacetamide (IA, 150 μM), or 4-hydroxynonenal (4-HNE, 200 μM) were inhibited by A96 (10 μM). n = 5 per condition. $p < 0.0001$ for agonists versus agonists + A96, two-way ANOVA with post hoc Bonferroni test.

(D) Ca^{2+} responses elicited by metabolites (200 μM) in HEK293 cells expressing Olfr558. Ionomycin (iono, 1 μM) was added at the end of each experiment to induce maximal Ca^{2+} responses. Black traces represent an average of all cells in the field shown in gray. Scale bar, 0.2 Fura-2 ratio, 50 s.

(E) Dose-response comparing isovalerate (blue), isobutyrate (purple), butyrate (orange), propionate (light blue), or acetate (green) represented as % of cells that responded to the indicated concentration of each compound. n = 6 per condition. EC_{50} for isovalerate was 8.92 μM with a 95% confidence interval of 7.32–10.51 μM.

(F) Isovalerate-evoked Ca^{2+} responses in EC cells. n = 5 per condition. $p < 0.001$ for control (vehicle-treated or empty Cas9-containing vector-infected organoids) versus cholera toxin (CTX), adenylyl cyclase inhibitor SQ22536 (10 μM), Ca^{2+} free extracellular solution, ω-agatoxin IVA (300 nM), Olfr558 knockout (KO). All data represented as mean ± SEM. n = 5–8 per condition, one-way ANOVA with post hoc Bonferroni test.

(G) Isovalerate (IVL, 200 μM)-evoked responses were absent in Olfr558 knockout (KO) ChgA-GFP organoids generated using CRISPR. Scale bar, 0.1 Fura-2 ratio, 50 s.

See also Figures S3 and S4.

Mechanism of EC Cell Activation by Chemical Irritants or Microbial Metabolites

Expression of TRPA1 channels is sufficient to account for sensitivity of EC cells to AITC and other electrophilic irritants. These responses were blocked by the selective antagonist A967079, further substantiating expression of functional TRPA1 channels by EC cells (Figure 2C).

To determine whether Olfr558 exhibits a pharmacological profile consistent with metabolite sensitivities observed in EC cells, we expressed mouse Olfr558 in HEK293 cells together with chimeric $G\alpha_{olf/15}$, which couples olfactory receptors to intracellular Ca^{2+} release as a proxy for receptor activity (Zhuang and Matsunami, 2008). Isovalerate evoked large Ca^{2+} responses in these cells, but not in $G\alpha_{olf/15}$-transfected controls lacking Olfr558

(Figures 2D and 2E). Consistent with native EC cell responses, isobutyrate or butyrate evoked smaller responses in fewer cells, while propionate or acetate were inactive (Figures 2D and 2E). Human Olfr558 exhibited similar metabolite sensitivities (Figure S4A). In EC cells, isovalerate-evoked responses were abolished by pretreatment with the $G\alpha_{olf/s}$ regulator cholera toxin or the adenylyl cyclase inhibitor SQ22536, but were not perturbed by inhibitors of other signaling cascades (Figure 2F). Furthermore, responses were not observed in Ca^{2+}-free extracellular solution and were significantly reduced by the P/Q-type Ca_V channel inhibitor ω-agatoxin IVA (Figure 2F). Together, these results suggest that isovalerate activates a $G\alpha_{olf/s}$-adenylyl cyclase signaling cascade in EC cells (akin to the canonical transduction pathway in olfactory epithelium), promoting Ca^{2+} influx through downstream Ca_V channels.

Finally, to ask if Olfr558 is required for isovalerate-induced responses in EC cells, we used CRISPR/Cas9 to disrupt the Olfr558 gene in ChgA-GFP intestinal organoids (Figures S4B and S4C). Doing so abolished isovalerate-evoked responses but did not affect AITC sensitivity, demonstrating that Olfr558 is required for isovalerate signaling in EC cells (Figures 2F, 2G, and S4D). Collectively, our data suggest that EC cells use Olfr558 to detect specific microbial metabolites present in gut and that the receptor is most selective for isovalerate.

Catecholamine Signal Transduction in EC Cells

Gut catecholamine levels, particularly norepinephrine, fluctuate with infection, inflammation, or altered sympathetic tone (Gabanyi et al., 2016). Consistent with a connection to sympathetic signaling and stress, EC cells were most sensitive to epinephrine and norepinephrine, which evoked large EC cell-specific responses (Figure S5A). Dopamine was ~100-fold less potent, suggesting that an adrenergic receptor(s) underlies catecholamine sensitivity in these cells. Indeed, yohimbine, an α2-adrenoreceptor subtype-selective antagonist, inhibited responses to all catecholamines (Figures 3A and 3B). Furthermore, EC cells were activated by clonidine, an α2-adrenoreceptor-selective agonist, but not by agonists for other adrenoreceptor subtypes (Figures S5B and S5C). Among α2-adrenoreceptors, only *Adrα2A* was transcriptionally expressed in EC cells, albeit at relatively low levels and in other intestinal epithelial cells (Figure S5D). However, Adrα2A immunoreactivity was specific to EC cells and localized to the basolateral surface, suggesting that protein expression is enriched in EC cells due to preferential translation or enhanced protein stability (Figure 3C). Tyrosine hydroxylase (TH), a marker for norepinephrine-producing sympathetic fibers, was localized adjacent to EC cells (Figure 3D), suggesting that sympathetic output can stimulate EC cells by acting on basolateral Adrα2A.

How does adrenergic signaling activate EC cells? Inhibition of $G\alpha_i$ by pertussis toxin blocked epinephrine-evoked Ca^{2+} responses (Figures S5E and S5F). Furthermore, responses were attenuated in the absence of extracellular Ca^{2+}, but Ca^{2+} influx was not dependent on Na_V or Ca_V channels since neither tetrodotoxin nor ω-agatoxin IVA abolished responses (Figures 3E and S5G). Another candidate transducer, namely TRPC4, is a Ca^{2+}-permeable channel that can be activated downstream of $G\alpha_i$-coupled receptors (Jeon et al., 2012) and is highly enriched in EC cells (Figure 2B). Indeed, the pan-TRPC blocker, 2-aminoethoxydiphenyl borate (2-APB), or the TRPC4-specific inhibitor, ML204, abolished epinephrine-evoked responses, whereas the TRPA1-selective inhibitor, A967079, had no effect (Figures 3E and S5H). These results suggest that TRPC4 contributes to the Ca^{2+}-permeable conductance stimulated downstream of adrenoreceptor activation in EC cells.

As further evidence that Adrα2A and TRPC4 can form a catecholamine-sensitive signaling cascade, we measured large epinephrine-evoked Ca^{2+} responses in HEK293 cells heterologously expressing both proteins, whereas no responses were seen in cells expressing Adrα2A or TRPC4 alone, or Adrα2A plus TRPC1, TRPC3, or TRPC6 (Figures S5I and S5J). We also observed large, ML204-sensitive epinephrine-evoked currents in HEK293 co-expressing Adrα2A and TRPC4, but not in cells individually expressing these proteins (Figures 3F–3H). Consistent with our results from EC cells implicating $G\alpha_i$-dependent signaling, these currents were blocked by pertussis toxin or by co-expression of a dominant-negative $G\alpha_i$ protein. Furthermore, co-expression of a constitutively active $G\alpha_i$ induced ML204-sensitive TRPC4 currents that occluded epinephrine-evoked responses (Figures 3F and 3H). Taken together, our results demonstrate that Adrα2A and TRPC4 mediate catecholamine sensitivity in EC cells via a $G\alpha_i$-dependent signaling cascade.

EC Cell Stimulation Promotes Ca_V-Dependent Serotonin Release

EC cells are serotonergic, but given their low abundance, serotonin release has typically been measured in bulk from intact tissue or model endocrine cell lines (Bertrand et al., 2008; Hagbom et al., 2011; Kim et al., 2001; Nozawa et al., 2009; Yano et al., 2015). To measure release from single EC cells directly, we monitored stimulus-evoked changes in cytoplasmic Ca^{2+} in GFP^+ EC cells within intact organoids, while simultaneously measuring whole-cell currents in adjacent biosensor cells expressing a serotonin-gated ion channel ($5\text{-}HT_3R$) (Figure 4A). Robust epinephrine-evoked Ca^{2+} responses in EC cells were quickly followed by large $5HT_3R$ currents in adjacent biosensor cells (Figure 4B). Epinephrine-dependent currents were comparable to maximal currents evoked by a saturating concentration of the $5HT_3R$ agonist, mCPBG (Figure 4B). High extracellular K^+ also evoked large Ca^{2+} responses and $5HT_3R$ currents, suggesting that EC cell depolarization is sufficient to induce serotonin release (Figure 4B). Importantly, when biosensor cells were relocated to GFP-negative epithelial cells, neither epinephrine nor K^+ elicited epithelial cell Ca^{2+} responses or $5HT_3R$ currents. As expected, direct activation of $5HT_3R$ by mCPBG evoked large currents in biosensor cells but did not elicit Ca^{2+} responses in EC cells (Figures 4A and 4B). Together, these data show that epinephrine promotes serotonin release directly and efficaciously from EC cells to produce local effects.

To determine how receptor-mediated signaling drives serotonin release, we perturbed major components of relevant transduction cascades while simultaneously measuring EC and biosensor cell responses. For example, yohimbine or ML204 blocked epinephrine-induced Ca^{2+} responses and $5HT_3R$ currents, confirming that the EC catecholamine signal transduction pathway controls serotonin release (Figures 4B, 4C, and 4F).

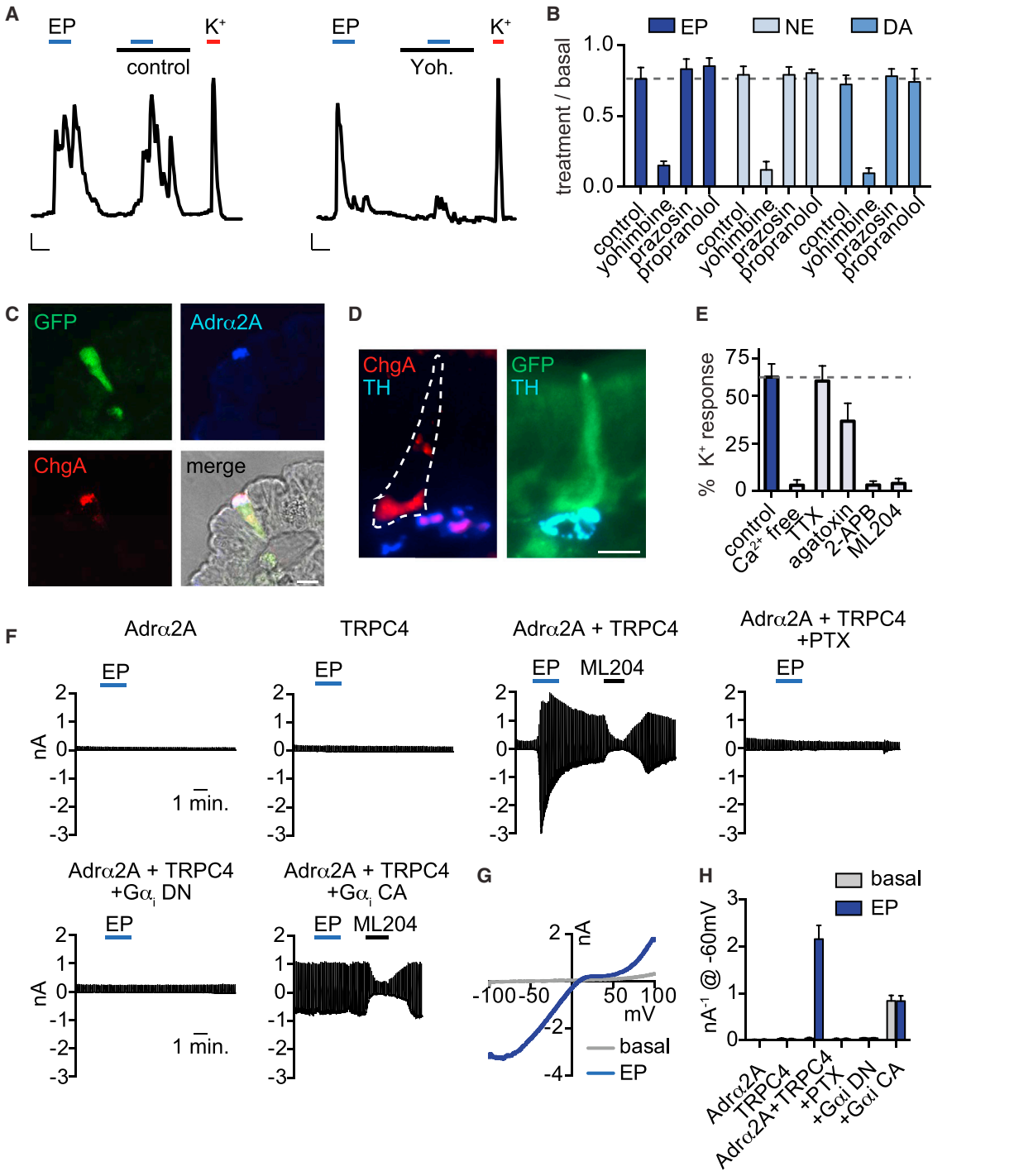

Figure 3. Adrα2A and TRPC4 Form a Catecholamine-Sensitive Signaling Cascade in Enterochromaffin Cells

(A) Epinephrine (EP, 1 μM)-evoked Ca^{2+} responses were blocked by the adrenoreceptor α2 (Adrα2) antagonist yohimbine (yoh, 5 μM). Scale bars, 0.1 Fura-2 ratio, 50 s.

(B) Average peak catecholamine responses were inhibited by the Adrα2 antagonist yohimbine, but not the Adrα1 antagonist prazosin (5 μM) or the Adrβ antagonist propranolol (5 μM). n = 5 per condition. $p < 0.0001$ for control versus yohimbine for EP (1 μM), norepinephrine (NE, 1 μM), dopamine (DA, 100 μM). Two-way ANOVA with post hoc Bonferroni test.

(C) Adrα2A (blue) localized to the basolateral side of EC cells (indicated by ChgA in red or GFP reporter) and was specific among intestinal epithelial cells. Scale bar, 10 μm.

(legend continued on next page)

Inhibition of Na_V channels with tetrodotoxin had no significant effect, whereas blockade of Ca^{2+} channels by ω-agatoxin IVA reduced Ca^{2+} responses in EC cells only slightly while completely abrogating $5HT_3R$ currents in biosensor cells (Figures 4C, 4F, S6A, and S6B). Similar results were seen with AITC (Figures 4D and 4F). Isovalerate also evoked EC cell Ca^{2+} responses that correlated with $5HT_3R$ currents (Figures 4E and 4F). In this case, both Ca^{2+} responses and $5HT_3R$ currents were markedly reduced by ω-agatoxin IVA (Figures 4E and 4F), consistent with the involvement of Ca_V channels in isovalerate-evoked EC cell Ca^{2+} responses (Figure 2F). Importantly, none of these inhibitors directly affected $5HT_3R$ currents (Figures S6C and S6D). Thus, Ca_V channels are required for serotonin release, likely mediating a local increase in intracellular Ca^{2+} near vesicular release sites, as observed for P/Q-type Ca_V channels in neuronal presynaptic terminals (Catterall et al., 2005b). Na_V channels are apparently not required for serotonin release, but may amplify responses to sub-threshold stimuli by generating action potentials.

EC Cells Regulate $5HT_3R$-Expressing Nerves via Synaptic-like Contacts

$5HT_3R$ is robustly expressed by intrinsic neurons of the gut within submucosal and myenteric plexi, as well as by a subset of primary afferent sensory nerve fibers, including some that innervate the intestinal villi (Tecott et al., 1995). Moreover, pharmacological experiments with isolated (ex vivo) ileum strips suggest that AITC-evoked release of serotonin from EC cells produces intestinal contractions in a $5HT_3R$-dependent manner (Nozawa et al., 2009). However, it is unclear whether such responses are mediated through diffuse, humoral spread of transmitter or a more direct, spatially restricted mechanism. In fact, previous anatomical studies have suggested that peptide hormone-producing intestinal endocrine cells form synapses with neurons (Bohórquez et al., 2015). Using a reporter mouse expressing GFP under control of the $5HT_3R$ promoter (Vucurovic et al., 2010), we confirmed that many $5HT_3R$-expressing nerve fibers innervate intestinal villi (Figure 5A). Moreover, $5HT_3R$-expressing fibers co-localized with synaptic markers, consistent with a neural origin (Figure S7A). Interestingly, we observed multiple instances where $5HT_3R$-expressing fibers appeared to make contact with the basolateral side of serotonin-expressing EC cells (Figure 5A). Because EC cells express presynaptic P/Q-type Ca_V channels, are enriched for gene ontology categories related to neurotransmitter secretion, and express transcripts for several presynaptic markers (Figures 5B and 5C), we wondered if this contact resembles a neural synapse. Indeed, EC cells demonstrated basolateral expression of the presynaptic marker, synapsin, and dense labeling of the postsynaptic marker, PSD-95, was observed immediately adjacent to EC cells (Figure 5D). Thus, EC cells are in close proximity with 5-HT_3R-expressing nerve fibers and appear to form synaptic-like structures for transmitting signals in a restricted, point-to-point manner.

To determine if EC cells regulate activity of sensory fibers, we recorded from single, low threshold mechanosensitive pelvic fibers that project deep into the colonic tissue and access the mucosal layer containing EC cells. Epithelial application of norepinephrine evoked large responses in afferent nerves that were abolished by the TRPC4 inhibitor, ML204 (Figure 6A). These responses were also blocked by the selective $5HT_3R$ antagonist, alosetron (Figure 6A), indicating that they are mediated by $5HT_3R$-expressing nerve fibers. Another EC cell agonist, isovalerate, evoked afferent nerve activity that was also blocked by alosetron (Figure 6A). Neither norepinephrine nor isovalerate directly activated isolated, retrogradely-traced colonic sensory dorsal root ganglion (DRG) neurons, many of which were sensitive to the $5HT_3R$-selective agonist, mCPBG (Figure 6B). Thus, norepinephrine and isovalerate modulate $5HT_3R$-expressing primary afferent nerve fibers via synaptically-coupled EC cells.

Chronic mechanical hypersensitivity contributes to the development of visceral pain syndromes, such as irritable bowel syndrome (Brierley and Linden, 2014). Interestingly, we found that epithelial application of norepinephrine (Figures 7A and S8A) or isovalerate (Figures 7B and S8B) markedly enhanced sensitivity of nerve fibers to mechanical stimulation of the colonic epithelium. Norepinephrine modulatory effects were blocked by ML204 and responses to norepinephrine or isovalerate were abolished by alosetron (Figures 7 and S8). These results are consistent with a role for EC cell-$5HT_3R$ signaling in regulating mechanical sensitivity of the gut.

DISCUSSION

EC Cells as Polymodal Sensors of Noxious Stimuli

We show that EC cells are chemosensors that detect stimuli from three distinct sources including (1) ingested chemicals, (2) commensal organisms, and (3) endogenous regulatory pathways. Sensitivity to these agents is specified by receptors and transduction mechanisms that also contribute to other sensory or neural signaling systems. For example, TRPA1 is a well-known somatosensory receptor for exogenous dietary irritants from mustard and allium plants, or endogenously produced inflammatory agents,

(D) Tyrosine hydroxylase (TH, blue), a marker for norepinephrine-producing sympathetic nerve fibers, localized on the basolateral side of EC cells (indicated by ChgA in red or GFP reporter). Scale bar, 10 μm.

(E) Pharmacological profile of EP responses. n = 7 per condition. $p < 0.0001$ for control versus Ca^{2+} free, TRPC inhibitor 2-APB (50 μM), TRPC4 inhibitor ML204 (10 μM); $p < 0.05$ for control versus ω-agatoxin IVA (300nM). One-way ANOVA with post hoc Bonferroni test.

(F) EP-elicited currents were elicited from HEK293 coexpressing Adrα2A and TRPC4, but not cells independently expressing Adrα2A or TRPC4. EP-elicited currents were inhibited by pertussis toxin (PTX, 200 ng/mL) or coexpression of dominant-negative (DN) $G\alpha_i$. Coexpression of constitutively-active (CA) $G\alpha_i$ induced ML204-sensitive activity that occluded EP-elicited currents.

(G) Representative current-voltage relationship shows the peak EP response (blue) and basal current (gray) from the representative cell expressing Adrα2A and TRPC4 shown in F.

(H) Average peak current amplitude recorded at −60 mV before (basal, gray) or during EP (blue) application. n = 6 per condition. All data represented as mean ± SEM. $p < 0.0001$ for basal versus epinephrine-evoked currents in Adrα2A and TRPC4, two-way ANOVA with post hoc Bonferroni test.

See also Figure S5.

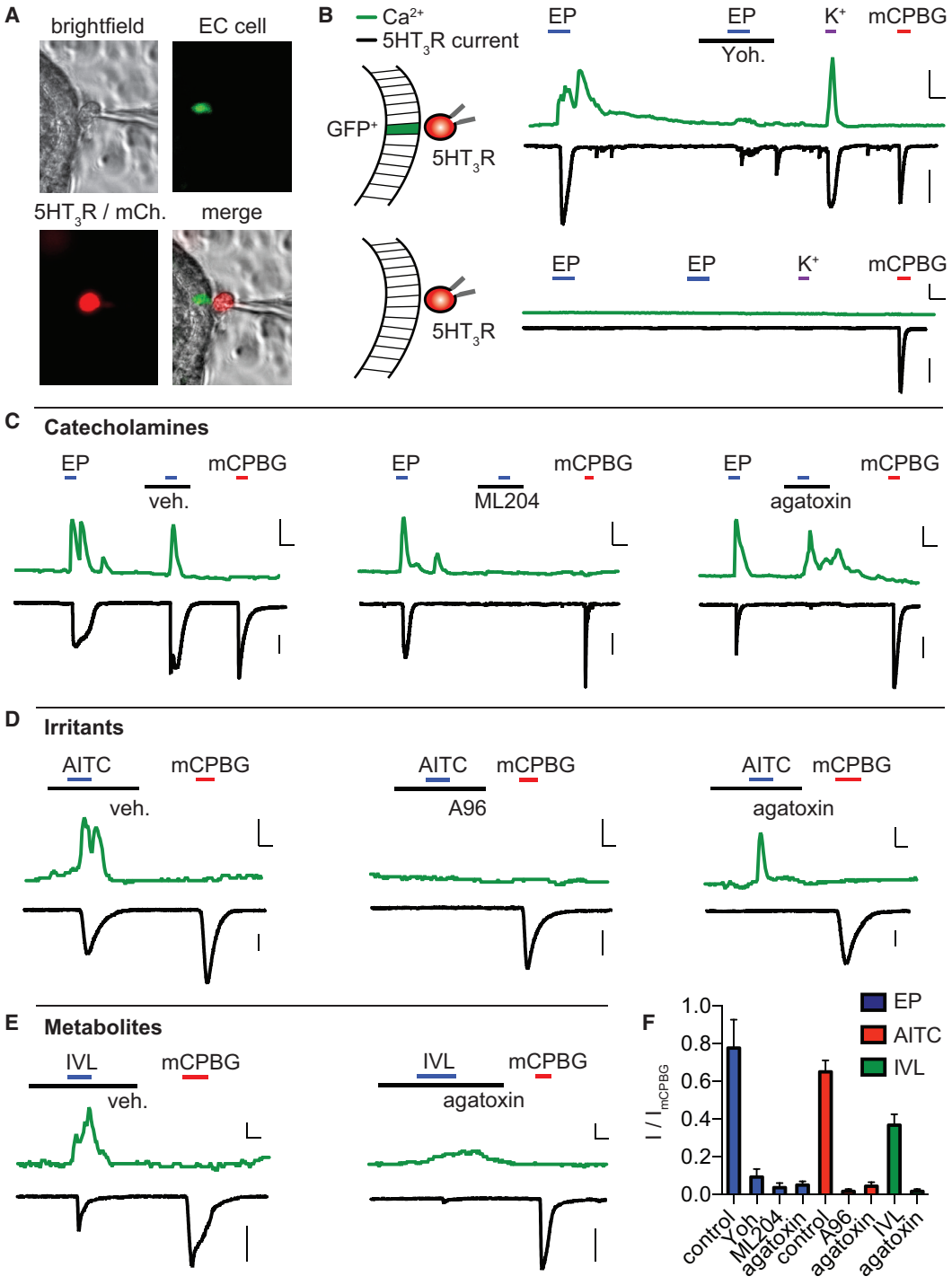

Figure 4. Enterochromaffin Cell Activation Mediates Ca_V-Dependent 5-HT Release

(A) Representative 5-HT "biosensor" experiment. $5HT_3R$-expressing HEK293 (mCherry, red) adjacent to an EC cell (GFP, green) for simultaneous Ca^{2+} measurements from EC cells and whole-cell current measurements from biosensor cells.

(B) Epinephrine (EP, 1 μM) or high extracellular K^+ induced a Ca^{2+} response in EC cells that correlated with a large $5HT_3R$ current in biosensor cells. EP responses were inhibited by yohimbine (yoh, 5 μM). The $5HT_3R$ agonist mCPBG (10 μM) elicited a large biosensor current, but no EC cell Ca^{2+} response. When biosensor cells were moved away from EC cells, neither epinephrine nor K^+ induced Ca^{2+} responses in GFP^- epithelial cells or biosensor currents, but mCPBG elicited a large $5HT_3R$ current. Scale bars, 0.6 Fura-2 ratio, 50 s, 500 pA.

(legend continued on next page)

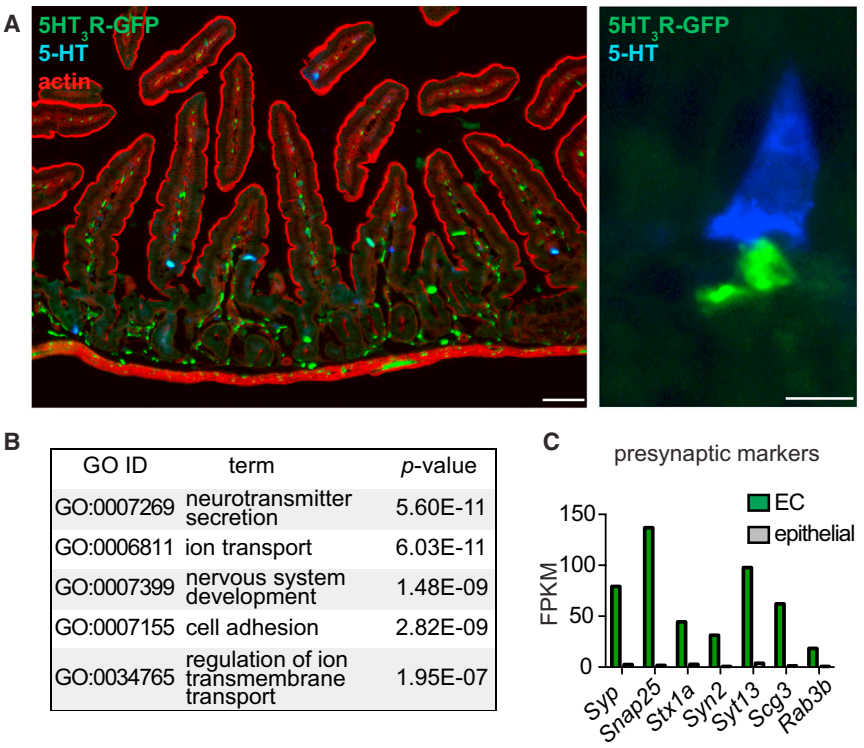

GO ID	term	*p*-value
GO:0007269	neurotransmitter secretion	5.60E-11
GO:0006811	ion transport	6.03E-11
GO:0007399	nervous system development	1.48E-09
GO:0007155	cell adhesion	2.82E-09
GO:0034765	regulation of ion transmembrane transport	1.95E-07

Figure 5. Enterochromaffin Cells Form Synaptic-like Contacts with $5HT_3R$-Expressing Nerve Fibers

(A) Left: representative jejunal cryosection showing $5HT_3R$-expressing fibers (green) innervating intestinal villi near serotonin-expressing EC cells (5-HT, blue) with actin staining (red) to demonstrate intestinal architecture. Scale bar, 50 μm. Right: representative image demonstrating proximity between a 5-HT-positive EC cell (blue) and $5HT_3R$-expressing fiber (green, basolateral side). Scale bar, 10 μm.

(B) Top five enriched Gene Ontology (GO) categories in EC cells compared with other intestinal epithelial cells.

(C) Presynaptic marker mRNA expression profile in EC cells (green) versus other intestinal epithelial cells (gray). Bars represent fragments per kilobase of exon per million fragments mapped (FPKM).

(D) A 5-μm section of intestinal epithelium showing a representative EC cell that expressed the presynaptic marker synapsin (blue, basolateral side) and made contact with a postsynaptic marker-positive fiber (PSD-95, red). Cell body is outlined (dashed white line). Three-dimensional rendering of EC cell (green) with synapsin-positive vesicles (blue) near postsynaptic-like structure (red). Scale bar, 10 μm.

See also Figure S7.

such as 4-hydroxynonenal, prostaglandins and other lipid-derived metabolites (Bautista et al., 2006; Trevisani et al., 2007). TRPA1 has been implicated in visceral hypersensitivity, but this has for the most part been attributed to its function on colonic nerve fibers (Brierley et al., 2009). Because the gut epithelium provides a barrier between the lumen and nerve fibers, our results, together with previous findings (Nozawa et al., 2009), now suggest that EC cell-localized TRPA1 serves as the primary detector of luminal irritants prior to direct sub-mucosal damage.

Effects of microbiota on the gastrointestinal system have been described at the organismal level, but underlying physiological mechanisms remain obscure (Schroeder and Bäckhed, 2016). For example, dietary fibers, proteins, and peptides are metabolized by commensal gut microbiota to produce volatile fatty acids, which in turn elicit diverse responses in the host through unknown mechanisms (Koh et al., 2016). Here, we identify one such metabolite, isovalerate, as a potent EC cell stimulus that modulates sensory neurons via EC cell-neural signaling. Although isovalerate accounts for only a minor percentage of total fatty acid metabolites, high levels are toxic and associated with visceral pain and other gastrointestinal disorders, such as post-infectious irritable bowel syndrome (Brierley and Linden, 2014; Farup et al., 2016; Tanaka et al., 1966). EC cells may act as sensors for such potentially harmful dysbiosis.

As with other specialized sensory systems, EC cell chemosensation may adapt to detect stimuli that are most salient to an animal's physiologic or environmental conditions, such as specific

(C) EP-evoked Ca^{2+} responses and $5HT_3R$ currents were not affected by vehicle but were blocked by the TRPC4 inhibitor ML204 (10 μM). The Ca_V inhibitor ω-agatoxin IVA (300 nM) slightly reduced Ca^{2+} responses and abolished $5HT_3R$ currents. Scale bars, 0.3 Fura-2 ratio, 50 s, 500 pA.

(D) AITC (150 μM)-evoked Ca^{2+} responses and $5HT_3R$ currents were blocked by the TRPA1 antagonist A967079 (A96, 10 μM). ω-agatoxin IVA (300 nM) did not significantly affect Ca^{2+} responses, but abolished $5HT_3R$ currents. Scale bars, 0.1 Fura-2 ratio, 25 s, 500pA.

(E) Isovalerate (IVL, 200 μM)-evoked Ca^{2+} responses and $5HT_3R$ currents. ω-agatoxin IVA (300 nM) inhibited Ca^{2+} responses and abolished $5HT_3R$ currents. Scale bars, 0.1 Fura-2 ratio, 25 s, 500 pA.

(F) Average agonist-evoked biosensor currents normalized to mCPBG-induced current (I_{mCPBG}). n = 4–5 per condition. Data represented as mean ± SEM. Responses to epinephrine (EP, blue), AITC (red), and isovalerate (IVL, green) in the presence of indicated antagonists. $p < 0.001$ for control versus treatments. One-way ANOVA with post hoc Tukey's test.

See also Figure S6.

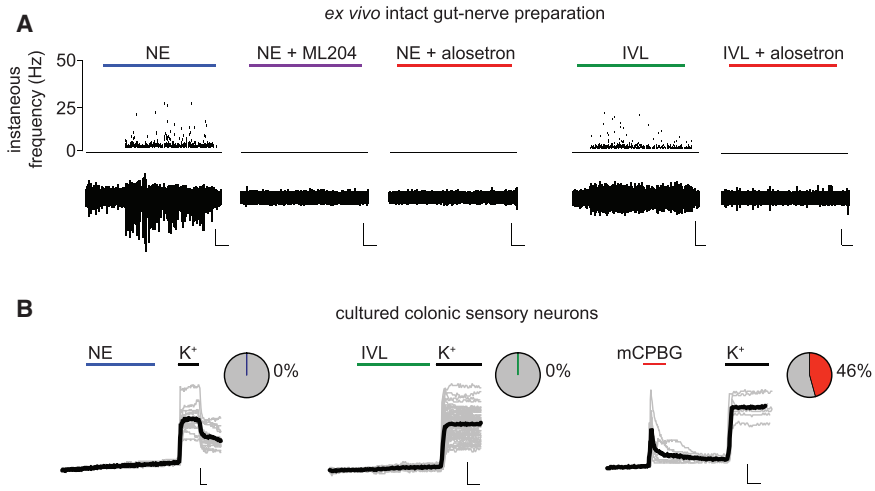

Figure 6. Enterochromaffin Cells Modulate 5HT$_3$R-Expressing Afferent Nerves

(A) Representative recordings from single mucosal afferent nerve fibers innervating intact colonic epithelium in an ex vivo preparation. Norepinephrine (NE, 1 μM) applied to the epithelium elicited chemosensory responses that were blocked by the TRPC4 inhibitor ML204 (10 μM) or the 5HT$_3$R antagonist alosetron (10 μM). Isovalerate (IVL, 200 μM) also evoked alosetron-sensitive afferent activity. Scale bars, 500 μV, 50 s. Representative of n = 8–9 per condition. $p < 0.0001$ for number of action potentials measured in response to NE (321.5 ± 55.4 spikes, 4/8 responsive fibers) versus NE + ML204 (0 spikes, 0/8 responsive fibers) or NE + alosetron (0 spikes, 0/9 responsive fibers), one-way ANOVA with post hoc Bonferroni test. $p < 0.01$ for number of action potentials measured in response to IVL (648.7 ± 339.3 spikes, 3/8 responsive fibers) versus IVL + alosetron (0 spikes, 0/8 responsive fibers).

(B) The 5HT$_3$R agonist mCPBG (10 μM), but not NE (1 μM) or isovalerate (IVL, 200 μM), evoked representative Ca^{2+} responses in retrogradely-labeled colonic sensory neurons isolated from lumbosacral dorsal root ganglia. All neurons quantified responded to high extracellular K^+. Black traces represent an average of all cells in the field shown in gray. Scale bar, 0.1 Fura-2 ratio, 60 s. Responsive neurons, n = 0/16 for NE, n = 0/62 for IVL, n = 16/35 for mCPBG.

diet, intestinal microbiota, etc. In this regard, it is interesting that mouse EC cells use Olfr558 as a sensor for specific microbial metabolites, whereas mRNA encoding a different repertoire of olfactory receptors has been detected in human EC cells (Braun et al., 2007), possibly reflecting species-specific sensory tuning to suit distinct commensal relationships. An important and fascinating future goal is to explore signaling diversity and plasticity in EC cells from different species or under a variety of physiologic or pathophysiologic states.

EC cells are also sensitive to endogenous regulatory molecules, including stress-associated catecholamine neurotransmitters. Interestingly, norepinephrine is a potent stimulus that upregulates proliferation, virulence, and adherence of various pathogenic bacteria to influence the course of infection (Everest, 2007). Norepinephrine-mediated stimulation of EC cells may be protective by activating neural pathways that promote gastrointestinal motility to expel infectious microbes, metabolites, or harmful chemicals. However, EC cell-afferent nerve fiber stimulation resulting from prolonged infection or injury may also be maladaptive, eliciting chronic visceral hypersensitivity. Consistent with a link between gut catecholamine signaling and visceral pain, polymorphisms or deletions in Adrα2A and TRPC4 genes, respectively, are associated with visceral pain syndromes (Kim et al., 2004; Westlund et al., 2014).

The gut is densely innervated by mechanosensory nerve fibers and enhanced afferent mechanical sensitivity is a hallmark of visceral pain (Brierley and Linden, 2014). We have shown that EC cell-neural chemosensory signaling cascades modulate mechanosensory function, establishing a direct mechanistic link between chemo- and mechanosensory elements in the gut. A recent study suggests that EC cells may themselves be mechanosensitive (Wang et al., 2017), but whether this contributes to mechanosensitivity of the gut is unknown.

EC Cell Signal Transduction

Our results demonstrate that EC cells detect specific chemosensory stimuli using independent signaling pathways that converge on P/Q-type presynaptic voltage-gated Ca^{2+} channels to facilitate transmitter release onto afferent nerve fibers. Interestingly, while the Ca^{2+}-permeable transduction channels TRPA1 and TRPC4 each support large increases in intracellular Ca^{2+}, their activation is apparently insufficient to elicit serotonin release since inhibition of Ca_V channels completely blocks transmitter release while only slightly decreasing global Ca^{2+} responses. Voltage-gated sodium channels are not required for stimulus-evoked release, although they likely amplify responses by generating action potentials, similar to what has been observed in hormone-secreting L-type enteroendocrine cells (Rogers et al., 2011). These and other results suggest that Ca_V channels mediate obligatory changes in local Ca^{2+}, likely near the site of transmitter release, demonstrating the importance of cellular excitability and voltage-gated channels in EC cell function. Future studies of EC cell synaptic proteins, vesicular pools and docking mechanisms, and state-dependent plasticity will enhance our understanding of this process. Crosstalk among signal transduction cascades may also come into play. For example, we have shown that $G\alpha_i$-coupled Adrα2A receptors activate TRPC4, but $G\alpha_q$-coupled receptors can also activate TRPC4, as well as TRPA1, providing opportunities for divergent and convergent effects of EC cell agonists on transmitter release.

Recent studies suggest a greater diversity of enteroendocrine cells than previously appreciated, arguing for the existence of genetically distinct EC cell subtypes (Diwakarla et al., 2017; Grün et al., 2015; Gunawardene et al., 2011). Indeed, we found that only a fraction of EC cells (7 of 62, Figure 2A) were GABA-responsive, indicative of some degree of functional specification. However, other compounds elicited cellular responses in nearly all EC cells (Figure 2A): AITC-evoked responses were

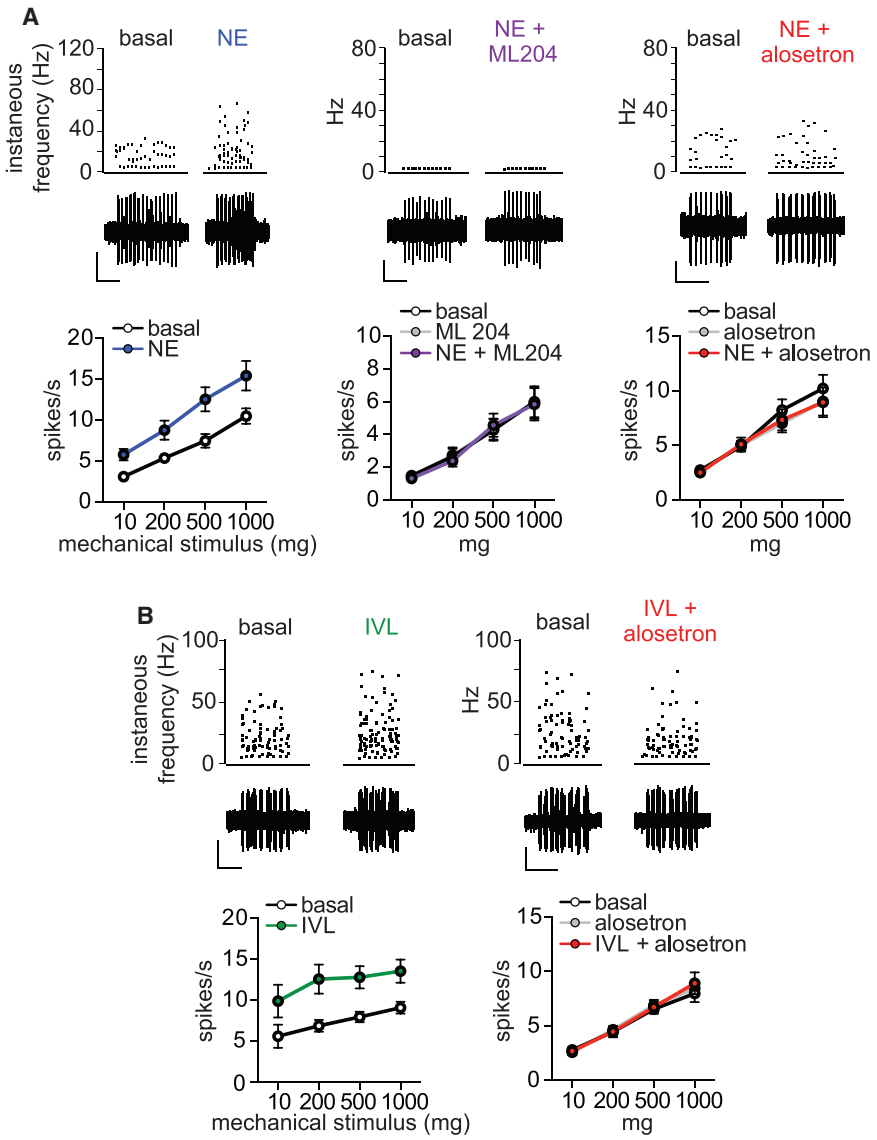

Figure 7. Enterochromaffin Cells Induce Mechanical Hypersensitivity of Colonic Afferents

(A) Representative mechanical responses from single low-threshold mechanoreceptive mucosal afferent fibers elicited by a 10 mg von Frey hair stimulus to epithelium. Mechanical responses were enhanced following epithelial treatment with norepinephrine (NE, 1 μM) and hypersensitivity was blocked by the TRPC4 inhibitor ML204 (10 μM) or $5HT_3R$ antagonist alosetron (10 μM). n = 8–9 per condition. Scale bars, 400 μV, 10 s. $p < 0.0001$ for contribution of treatment to series variance for NE versus basal and no significant difference with NE + ML204 or alosetron, two-way ANOVA with post hoc Bonferroni test.

(B) Afferent mechanosensory responses were enhanced following epithelial treatment with isovalerate (IVL, 200 μM) and hypersensitivity was blocked by alosetron (10 μM). A 500 mg von Frey hair was used as an epithelial mechanical stimulus for representative traces. n = 8–9 per condition. Scale bars, 500 μV, 10 s. $p < 0.0001$ for contribution of treatment to series variance for IVL versus basal and no significant difference with IVL + alosetron, two-way ANOVA with post hoc Bonferroni test. All data represented as mean ± SEM.

See also Figure S8.

observed in 15 of 15 high K^+-responsive cells, norepinephrine responses in 30 of 30 cells, and isovalerate responses in 16 of 17 cells, suggesting that some functional attributes are conserved across most, if not all, putative EC cell subsets. Distinct enteroendocrine cells are derived from a common precursor; therefore, it is possible particular sensory receptors or pathways are conserved among subtypes. Indeed, TRPA1 activity has been observed in L-cells to mediate GLP-1 release (Emery et al., 2015).

EC Cell-Neural Communication

Signaling diversity or plasticity may also manifest at the level of neural circuitry. Our data show that EC cells make contact with $5HT_3R$-expressing nerve fibers to mediate relatively local effects of serotonin. Consistent with previous reports (Aiken and Roth, 1992; Heitz et al., 1976), we found that EC cells are peptidergic, and substance P expression is most prevalent in cells within crypts, decreasing upward along the crypt-villus axis (Figures S7B–S7D). Thus, EC cells may also release peptide transmitters to regulate synaptically-coupled sensory neurons. Moreover, hormone-producing enteroendocrine cells also form synaptic connections with nerve fibers (Bohórquez et al., 2015), although it is unknown if these neurons are of enteric or sensory origin. Therefore, sensory molecules could act on multiple enteroendocrine cell types to induce diverse signals (peptide hormones, serotonin) to regulate afferent nerve activity, conceivably transmitting specialized information through activation of specific fiber types or differential modulation of neural activity (Gribble and Reimann, 2016). Furthermore, discrete subclasses of DRG or vagal sensory nerves may communicate with specific resident EC cell populations (Williams et al., 2016). Finally, EC cell-derived serotonin may, in some cases, act on enteric neurons, immune cells, or be taken up by circulating platelets to mediate diverse actions within or outside of the gut (Gershon, 2013; Veiga-Fernandes and Mucida, 2016).

EC Cells and GI Disorders

Alterations in EC cell-derived serotonin have been implicated in GI dysmotility, nausea, and visceral hypersensitivity disorders (Gershon, 2013; Mawe and Hoffman, 2013), and medications affecting norepinephrine or serotonin levels are associated with beneficial peripheral gut effects, such as relaxed fasting

colonic muscle tone and reduction in mechanical hypersensitivity (Chial et al., 2003; Winston et al., 2010). Indeed, $5HT_3$R-targeted therapeutics are used to treat chemotherapy-induced emesis, chronic nausea, and other visceral pain disorders (Mawe and Hoffman, 2013). Microbial metabolites also influence GI status and recent studies have noted beneficial effects of probiotics and differences in volatile fatty acids in patients with irritable bowel syndrome (Didari et al., 2015; Treem et al., 1996). Furthermore, intestinal inflammation is a key risk factor for the development of irritable bowel syndrome, and inflammatory molecules are associated with enhanced mechanical hypersensitivity of the gut (Brierley and Linden, 2014).

Our findings highlight EC cells as polymodal chemosensors that integrate extrinsic and intrinsic signals within the gut and convey this information to the nervous system. By exploiting intestinal organoid technology to access these rare, but important cells, we have gleaned new mechanistic insights into their function, which should facilitate EC cell-targeted therapeutics to treat irritable bowel syndrome and other disorders associated with gut hypersensitivity and pathophysiology.

STAR★METHODS

Detailed methods are provided in the online version of this paper and include the following:

- KEY RESOURCES TABLE
- METHODS
  - Contact for reagent and resource sharing
- EXPERIMENTAL MODEL AND SUBJECT DETAILS
  - Animals
  - Intestinal organoids
  - Cultured cells
- METHOD DETAILS
  - CRISPR-mediated gene disruption
  - Electrophysiology
  - Calcium imaging
  - Transcriptome sequencing and analysis
  - Histology
  - Single nerve fiber recordings of pelvic colonic mucosal afferents
- QUANTIFICATION AND STATISTICAL ANALYSIS
- DATA AVAILABILITY

SUPPLEMENTAL INFORMATION

Supplemental Information includes eight figures and can be found with this article online at http://dx.doi.org/10.1016/j.cell.2017.05.034.

AUTHOR CONTRIBUTIONS

N.W.B., J.R.B., D.B.L., C.Z., H.A.I., and D.J. contributed to molecular and anatomical studies of EC cells. J.C., T.A.O.D., and S.M.B. contributed to colonic afferent studies. All authors were involved with writing or reviewing the manuscript.

ACKNOWLEDGMENTS

We thank J. Poblete and H. Escusa for technical assistance, S. Elmes for help with FACS, M. Fischbach for helpful discussion, and R. Nicoll for critical reading of the manuscript. This work was supported by a NIH Institutional Research Service Award to the UCSF CVRI (T32HL007731 to N.W.B.), a Howard Hughes Medical Institute Fellowship of the Life Sciences Research Foundation (N.W.B.), a Simons Foundation Postdoctoral Fellowship to the Jane Coffin Childs Memorial Fund 61-1559 to D.B.L., grants from the NIH (R01 NS081115 and R01 NS055299 to D.J., R01 DK099722 to H.A.I., and K12 HD072222 and K08 DK106577 to J.R.B.), the American Diabetes Association (714MI08 to H.A.I.), and the National Health and Medical Research Council of Australia (APP1083480 to S.M.B.). S.M.B. is a NHMRC R.D. Wright Biomedical Research Fellow (APP1126378).

Received: January 8, 2017
Revised: May 5, 2017
Accepted: May 22, 2017
Published: June 22, 2017

REFERENCES

Aiken, K.D., and Roth, K.A. (1992). Temporal differentiation and migration of substance P, serotonin, and secretin immunoreactive enteroendocrine cells in the mouse proximal small intestine. Dev. Dyn. *194*, 303–310.

Andrews, S. (2010). FastQC: A quality control tool for high throughput sequence data. Babraham Bioinformatics, http://www.bioinformatics.babraham.ac.uk/projects/fastqc/.

Audouze, K., Tromelin, A., Le Bon, A.M., Belloir, C., Petersen, R.K., Kristiansen, K., Brunak, S., and Taboureau, O. (2014). Identification of odorant-receptor interactions by global mapping of the human odorome. PLoS ONE *9*, e93037.

Bautista, D.M., Jordt, S.E., Nikai, T., Tsuruda, P.R., Read, A.J., Poblete, J., Yamoah, E.N., Basbaum, A.I., and Julius, D. (2006). TRPA1 mediates the inflammatory actions of environmental irritants and proalgesic agents. Cell *124*, 1269–1282.

Bertrand, P.P., Hu, X., Mach, J., and Bertrand, R.L. (2008). Serotonin (5-HT) release and uptake measured by real-time electrochemical techniques in the rat ileum. Am. J. Physiol. Gastrointest. Liver Physiol. *295*, G1228–G1236.

Bohórquez, D.V., Shahid, R.A., Erdmann, A., Kreger, A.M., Wang, Y., Calakos, N., Wang, F., and Liddle, R.A. (2015). Neuroepithelial circuit formed by innervation of sensory enteroendocrine cells. J. Clin. Invest. *125*, 782–786.

Braun, T., Voland, P., Kunz, L., Prinz, C., and Gratzl, M. (2007). Enterochromaffin cells of the human gut: sensors for spices and odorants. Gastroenterology *132*, 1890–1901.

Brierley, S.M., and Linden, D.R. (2014). Neuroplasticity and dysfunction after gastrointestinal inflammation. Nat. Rev. Gastroenterol. Hepatol. *11*, 611–627.

Brierley, S.M., Jones, R.C., 3rd, Gebhart, G.F., and Blackshaw, L.A. (2004). Splanchnic and pelvic mechanosensory afferents signal different qualities of colonic stimuli in mice. Gastroenterology *127*, 166–178.

Brierley, S.M., Hughes, P.A., Page, A.J., Kwan, K.Y., Martin, C.M., O'Donnell, T.A., Cooper, N.J., Harrington, A.M., Adam, B., Liebregts, T., et al. (2009). The ion channel TRPA1 is required for normal mechanosensation and is modulated by algesic stimuli. Gastroenterology *137*, 2084–2095.e3.

Buffalo, V. (2011). Scythe—A very simple adapter trimmer (San Francisco: Github).

Catterall, W.A., Goldin, A.L., and Waxman, S.G. (2005a). International Union of Pharmacology. XLVII. Nomenclature and structure-function relationships of voltage-gated sodium channels. Pharmacol. Rev. *57*, 397–409.

Catterall, W.A., Perez-Reyes, E., Snutch, T.P., and Striessnig, J. (2005b). International Union of Pharmacology. XLVIII. Nomenclature and structure-function relationships of voltage-gated calcium channels. Pharmacol. Rev. *57*, 411–425.

Chial, H.J., Camilleri, M., Ferber, I., Delgado-Aros, S., Burton, D., McKinzie, S., and Zinsmeister, A.R. (2003). Effects of venlafaxine, buspirone, and placebo on colonic sensorimotor functions in healthy humans. Clin. Gastroenterol. Hepatol. *1*, 211–218.

Didari, T., Mozaffari, S., Nikfar, S., and Abdollahi, M. (2015). Effectiveness of probiotics in irritable bowel syndrome: Updated systematic review with meta-analysis. World J. Gastroenterol. *21*, 3072–3084.

Diwakarla, S., Fothergill, L.J., Fakhry, J., Callaghan, B., and Furness, J.B. (2017). Heterogeneity of enterochromaffin cells within the gastrointestinal tract. Neurogastroenterol. Motil. *29*, http://dx.doi.org/10.1111/nmo.13101.

Doihara, H., Nozawa, K., Kojima, R., Kawabata-Shoda, E., Yokoyama, T., and Ito, H. (2009). QGP-1 cells release 5-HT via TRPA1 activation; a model of human enterochromaffin cells. Mol. Cell. Biochem. *331*, 239–245.

Emery, E.C., Diakogiannaki, E., Gentry, C., Psichas, A., Habib, A.M., Bevan, S., Fischer, M.J., Reimann, F., and Gribble, F.M. (2015). Stimulation of GLP-1 secretion downstream of the ligand-gated ion channel TRPA1. Diabetes *64*, 1202–1210.

Engelstoft, M.S., Lund, M.L., Grunddal, K.V., Egerod, K.L., Osborne-Lawrence, S., Poulsen, S.S., Zigman, J.M., and Schwartz, T.W. (2015). Research resource: a chromogranin a reporter for serotonin and histamine secreting enteroendocrine cells. Mol. Endocrinol. *29*, 1658–1671.

Everest, P. (2007). Stress and bacteria: microbial endocrinology. Gut *56*, 1037–1038.

Farup, P.G., Rudi, K., and Hestad, K. (2016). Faecal short-chain fatty acids - a diagnostic biomarker for irritable bowel syndrome? BMC Gastroenterol. *16*, 51.

Flegel, C., Manteniotis, S., Osthold, S., Hatt, H., and Gisselmann, G. (2013). Expression profile of ectopic olfactory receptors determined by deep sequencing. PLoS ONE *8*, e55368.

Fukumoto, S., Tatewaki, M., Yamada, T., Fujimiya, M., Mantyh, C., Voss, M., Eubanks, S., Harris, M., Pappas, T.N., and Takahashi, T. (2003). Short-chain fatty acids stimulate colonic transit via intraluminal 5-HT release in rats. Am. J. Physiol. Regul. Integr. Comp. Physiol. *284*, R1269–R1276.

Furness, J.B., Rivera, L.R., Cho, H.J., Bravo, D.M., and Callaghan, B. (2013). The gut as a sensory organ. Nat. Rev. Gastroenterol. Hepatol. *10*, 729–740.

Gabanyi, I., Muller, P.A., Feighery, L., Oliveira, T.Y., Costa-Pinto, F.A., and Mucida, D. (2016). Neuro-immune interactions drive tissue programming in intestinal macrophages. Cell *164*, 378–391.

Gershon, M.D. (2013). 5-Hydroxytryptamine (serotonin) in the gastrointestinal tract. Curr. Opin. Endocrinol. Diabetes Obes. *20*, 14–21.

Gribble, F.M., and Reimann, F. (2016). Enteroendocrine cells: chemosensors in the intestinal epithelium. Annu. Rev. Physiol. *78*, 277–299.

Grün, D., Lyubimova, A., Kester, L., Wiebrands, K., Basak, O., Sasaki, N., Clevers, H., and van Oudenaarden, A. (2015). Single-cell messenger RNA sequencing reveals rare intestinal cell types. Nature *525*, 251–255.

Gunawardene, A.R., Corfe, B.M., and Staton, C.A. (2011). Classification and functions of enteroendocrine cells of the lower gastrointestinal tract. Int. J. Exp. Pathol. *92*, 219–231.

Hagbom, M., Istrate, C., Engblom, D., Karlsson, T., Rodriguez-Diaz, J., Buesa, J., Taylor, J.A., Loitto, V.M., Magnusson, K.E., Ahlman, H., et al. (2011). Rotavirus stimulates release of serotonin (5-HT) from human enterochromaffin cells and activates brain structures involved in nausea and vomiting. PLoS Pathog. *7*, e1002115.

Heitz, P., Polak, J.M., Timson, D.M., and Pearse, A.G.E. (1976). Enterochromaffin cells as the endocrine source of gastrointestinal substance P. Histochemistry *49*, 343–347.

Huang, da W., Sherman, B.T., and Lempicki, R.A. (2009). Systematic and integrative analysis of large gene lists using DAVID bioinformatics resources. Nat Protoc. *4*, 44–57.

Ishii, T., Omura, M., and Mombaerts, P. (2004). Protocols for two- and three-color fluorescent RNA in situ hybridization of the main and accessory olfactory epithelia in mouse. J. Neurocytol. *33*, 657–669.

Jeon, J.P., Hong, C., Park, E.J., Jeon, J.H., Cho, N.H., Kim, I.G., Choe, H., Muallem, S., Kim, H.J., and So, I. (2012). Selective Gαi subunits as novel direct activators of transient receptor potential canonical (TRPC)4 and TRPC5 channels. J. Biol. Chem. *287*, 17029–17039.

Joshi, N. (2011). Sickle—A windowed adaptive trimming tool for FASTQ files using quality (San Francisco: GitHub).

Kim, D., Pertea, G., Trapnell, C., Pimentel, H., Kelley, R., and Salzberg, S.L. (2013). TopHat2: accurate alignment of transcriptomes in the presence of insertions, deletions and gene fusions. Genome Biol. *14*, R36.

Kim, M., Cooke, H.J., Javed, N.H., Carey, H.V., Christofi, F., and Raybould, H.E. (2001). D-glucose releases 5-hydroxytryptamine from human BON cells as a model of enterochromaffin cells. Gastroenterology *121*, 1400–1406.

Kim, H.J., Camilleri, M., Carlson, P.J., Cremonini, F., Ferber, I., Stephens, D., McKinzie, S., Zinsmeister, A.R., and Urrutia, R. (2004). Association of distinct alpha(2) adrenoceptor and serotonin transporter polymorphisms with constipation and somatic symptoms in functional gastrointestinal disorders. Gut *53*, 829–837.

Koh, A., De Vadder, F., Kovatcheva-Datchary, P., and Bäckhed, F. (2016). From dietary fiber to host physiology: short-chain fatty acids as key bacterial metabolites. Cell *165*, 1332–1345.

Maricq, A.V., Peterson, A.S., Brake, A.J., Myers, R.M., and Julius, D. (1991). Primary structure and functional expression of the 5HT3 receptor, a serotonin-gated ion channel. Science *254*, 432–437.

Mawe, G.M., and Hoffman, J.M. (2013). Serotonin signalling in the gut–functions, dysfunctions and therapeutic targets. Nat. Rev. Gastroenterol. Hepatol. *10*, 473–486.

Nozawa, K., Kawabata-Shoda, E., Doihara, H., Kojima, R., Okada, H., Mochizuki, S., Sano, Y., Inamura, K., Matsushime, H., Koizumi, T., et al. (2009). TRPA1 regulates gastrointestinal motility through serotonin release from enterochromaffin cells. Proc. Natl. Acad. Sci. USA *106*, 3408–3413.

Öhman, L., Törnblom, H., and Simrén, M. (2015). Crosstalk at the mucosal border: importance of the gut microenvironment in IBS. Nat. Rev. Gastroenterol. Hepatol. *12*, 36–49.

Priori, D., Colombo, M., Clavenzani, P., Jansman, A.J.M., Lallès, J.P., Trevisi, P., and Bosi, P. (2015). The olfactory receptor OR51E1 is present along the gastrointestinal tract of pigs, co-localizes with enteroendocrine cells and is modulated by intestinal microbiota. PLoS ONE *10*, e0129501.

Racké, K., and Schwörer, H. (1993). Characterization of the role of calcium and sodium channels in the stimulus secretion coupling of 5-hydroxytryptamine release from porcine enterochromaffin cells. Naunyn Schmiedebergs Arch. Pharmacol. *347*, 1–8.

Raghupathi, R., Duffield, M.D., Zelkas, L., Meedeniya, A., Brookes, S.J., Sia, T.C., Wattchow, D.A., Spencer, N.J., and Keating, D.J. (2013). Identification of unique release kinetics of serotonin from guinea-pig and human enterochromaffin cells. J. Physiol. *591*, 5959–5975.

Rogers, G.J., Tolhurst, G., Ramzan, A., Habib, A.M., Parker, H.E., Gribble, F.M., and Reimann, F. (2011). Electrical activity-triggered glucagon-like peptide-1 secretion from primary murine L-cells. J Physiol. *589*, 1081–1093.

Saito, H., Chi, Q., Zhuang, H., Matsunami, H., and Mainland, J.D. (2009). Odor coding by a Mammalian receptor repertoire. Sci Signal. *2*, ra9.

Sanjana, N.E., Shalem, O., and Zhang, F. (2014). Improved vectors and genome-wide libraries for CRISPR screening. Nat. Methods *11*, 783–784.

Sato, T., Vries, R.G., Snippert, H.J., van de Wetering, M., Barker, N., Stange, D.E., van Es, J.H., Abo, A., Kujala, P., Peters, P.J., and Clevers, H. (2009). Single Lgr5 stem cells build crypt-villus structures in vitro without a mesenchymal niche. Nature *459*, 262–265.

Schroeder, B.O., and Bäckhed, F. (2016). Signals from the gut microbiota to distant organs in physiology and disease. Nat. Med. *22*, 1079–1089.

Tanaka, K., Budd, M.A., Efron, M.L., and Isselbacher, K.J. (1966). Isovaleric acidemia: a new genetic defect of leucine metabolism. Proc. Natl. Acad. Sci. USA *56*, 236–242.

Tecott, L., Shtrom, S., and Julius, D. (1995). Expression of a serotonin-gated ion channel in embryonic neural and nonneural tissues. Mol. Cell. Neurosci. *6*, 43–55.

Trapnell, C., Hendrickson, D.G., Sauvageau, M., Goff, L., Rinn, J.L., and Pachter, L. (2013). Differential analysis of gene regulation at transcript resolution with RNA-seq. Nat Biotechnol *31*, 46–53.

Trapnell, C., Williams, B.A., Pertea, G., Mortazavi, A., Kwan, G., van Baren, M.J., Salzberg, S.L., Wold, B.J., and Pachter, L. (2010). Transcript assembly and quantification by RNA-Seq reveals unannotated transcripts and isoform switching during cell differentiation. Nat Biotechnol. *28*, 511–515.

Treem, W.R., Ahsan, N., Kastoff, G., and Hyams, J.S. (1996). Fecal short-chain fatty acids in patients with diarrhea-predominant irritable bowel syndrome: in vitro studies of carbohydrate fermentation. J. Pediatr. Gastroenterol. Nutr. *23*, 280–286.

Trevisani, M., Siemens, J., Materazzi, S., Bautista, D.M., Nassini, R., Campi, B., Imamachi, N., Andrè, E., Patacchini, R., Cottrell, G.S., et al. (2007). 4-Hydroxynonenal, an endogenous aldehyde, causes pain and neurogenic inflammation through activation of the irritant receptor TRPA1. Proc. Natl. Acad. Sci. USA *104*, 13519–13524.

Veiga-Fernandes, H., and Mucida, D. (2016). Neuro-Immune Interactions at Barrier Surfaces. Cell *165*, 801–811.

Vucurovic, K., Gallopin, T., Ferezou, I., Rancillac, A., Chameau, P., van Hooft, J.A., Geoffroy, H., Monyer, H., Rossier, J., and Vitalis, T. (2010). Serotonin 3A receptor subtype as an early and protracted marker of cortical interneuron subpopulations. Cereb. Cortex *20*, 2333–2347.

Wang, F., Knutson, K., Alcaino, C., Linden, D.R., Gibbons, S.J., Kashyap, P., Grover, M., Oeckler, R., Gottlieb, P.A., Li, H.J., et al. (2017). Mechanosensitive ion channel Piezo2 is important for enterochromaffin cell response to mechanical forces. J. Physiol. *595*, 79–91.

Westlund, K.N., Zhang, L.P., Ma, F., Nesemeier, R., Ruiz, J.C., Ostertag, E.M., Crawford, J.S., Babinski, K., and Marcinkiewicz, M.M. (2014). A rat knockout model implicates TRPC4 in visceral pain sensation. Neuroscience *262*, 165–175.

Williams, E.K., Chang, R.B., Strochlic, D.E., Umans, B.D., Lowell, B.B., and Liberles, S.D. (2016). Sensory Neurons that Detect Stretch and Nutrients in the Digestive System. Cell *166*, 209–221.

Winston, J.H., Xu, G.Y., and Sarna, S.K. (2010). Adrenergic stimulation mediates visceral hypersensitivity to colorectal distension following heterotypic chronic stress. Gastroenterology *138*, 294–304.

Yano, J.M., Yu, K., Donaldson, G.P., Shastri, G.G., Ann, P., Ma, L., Nagler, C.R., Ismagilov, R.F., Mazmanian, S.K., and Hsiao, E.Y. (2015). Indigenous bacteria from the gut microbiota regulate host serotonin biosynthesis. Cell *161*, 264–276.

Zhuang, H., and Matsunami, H. (2008). Evaluating cell-surface expression and measuring activation of mammalian odorant receptors in heterologous cells. Nat. Protoc. *3*, 1402–1413.

STAR★METHODS

KEY RESOURCES TABLE

REAGENT or RESOURCE	SOURCE	IDENTIFIER
Antibodies		
tyrosine hydroxylase	Millipore	Cat# AB152; RRID: AB_390204
PSD-95	Neuromab	Cat# 75-348; RRID: AB_2315909
lysozyme	Dako	Cat# EC 3.2.1.17; RRID: AB_2341231
GLP-1	Abcam	Cat# ab26278; RRID: AB_470838
substance P	Penninsula	T-4106
chromogranin A	Santa Cruz	Cat# Sc-1488; RRID: 2276319
serotonin	Immunostar	Cat# 24446; RRID: AB_572215
synapsin	Gift from R. Edwards	N/A
Adra2A	Affinity BioReagents	PA1-048
Anti-Digoxigenin-AP, Fab fragments	Sigma	11093274910
Anti-Fluorescein-POD, Fab fragments	Sigma	11426346910
Bacterial and Virus Strains		
plentiCRISPR-Olfr558	This paper	N/A
Chemicals, Peptides, and Recombinant Proteins		
CHIR99021	Sigma	SML1046
nicotinamide	Sigma	N0636
Y-27632	Sigma	Y0503
1-(m-chlorophenyl)-biguanide	Sigma	C144
allyl isothiocyanate	Sigma	377430
N-butyryl-L-Homoserine lactone	Cayman Chemical	10007898
N-hexanoyl-L-Homoserine lactone	Cayman Chemical	10007896
N-3-oxo-dodecanoyl-L-Homoserine lactone	Cayman Chemical	10007895
N-Formylmethionine-leucyl-phenylalanine	Sigma	F3506
E. Coli lipopolysaccharide	Sigma	L6529
indole	Sigma	I3408
propionate	Sigma	P1880
acetate	Sigma	S2889
butyrate	Sigma	B5887
isobutyrate	Sigma	I1754
isovalerate	Sigma	129542
deoxycholate	Sigma	D6750
substance P	Tocris	1156
histamine	Sigma	H7250
glutamate	Tocris	0218
tryptamine	Sigma	193747
serotonin	Sigma	H9523
glycine	Tocris	0219
gamma-aminobutyric acid	Tocris	0344
dopamine	Tocris	3548
epinephrine	Sigma	E4642
norepinephrine	Tocris	5169
tetrodotoxin	R&D Systems	1078
nifedipine	Alomone Labs	N-120

(*Continued on next page*)

Continued

REAGENT or RESOURCE	SOURCE	IDENTIFIER
ω-agatoxin IVA	Tocris	2799
ω-conotoxin	Tocris	1085
mibefradil	Tocris	2198
yohimbine	Tocris	1127
isoproterenol	Tocris	1747
prazosin	Tocris	0623
clonidine	Tocris	0690
propranolol	Tocris	0624
phenylephrine	Tocris	2838
U73122	Tocris	1268
gallein	Tocris	3090
pertussis toxin	Sigma	P7208
cholera toxin	Sigma	C8052
2-aminoethoxydiphenyl borate	Sigma	D9754
ML204	Tocris	4732
4-hydroxynonenal	Cayman Chemical	32100
alosetron	Selleckchem	S4694
capsaicin	Tocris	0462
menthol	Sigma	M2772
icilin	Tocris	1531
Critical Commercial Assays		
SMART-Seq v4 Ultra Low Input RNA Kit for Sequencing	Clontech	634888
Low Input Library Prep Kit	Clontech	634899
Agilent RNA 600 Pico Kit	Agilent	5067-1513
Deposited Data		
Deep sequencing data	This paper	GEO: GSE98794
Experimental Models: Cell Lines		
HEK293T	ATCC	CRL-3216
R-Spondin expressing cells	Gift from N. Shroyer, Baylor College of Medicine	N/A
Experimental Models: Organisms/Strains		
Mouse: ChgA-GFP reporter	Engelstoft et al., 2015	N/A
Mouse: $5HT_3R$-GFP reporter mice	Vucurovic et al., 2010	N/A
Oligonucleotides		
Olfr558 gRNA forward (5′ to 3′): CACCGagcacagtggcatgccgtag	This paper	N/A
Olfr558 gRNA reverse: AAACctacggcatgccactgtgctC	This paper	N/A
Olfr558 sequencing forward: ctttgcatgctttctggcct	This paper	N/A
Olfr558 sequencing reverse: tgcaggtgttcttccattcca	This paper	N/A
Recombinant DNA		
Plasmid: human Adra2A	Genscript	OHu19050
Plasmid: dominant negative Gai2	cDNA Resource Center	GNAI2000T0
Plasmid: constituently active Gai2	cDNA Resource Center	GNAI2000C0
Plasmid: TRPC4	Jeon et al., 2012	N/A

(*Continued on next page*)

Continued

REAGENT or RESOURCE	SOURCE	IDENTIFIER
Plasmid: TRPC1	This paper	N/A
Plasmid: TRPC3	This paper	N/A
Plasmid: TRPC6	This paper	N/A
Plasmid: RTP1S	Zhuang and Matsunami, 2008	N/A
Plasmid: Ric8b	Zhuang and Matsunami, 2008	N/A
Plasmid: Gaolf/15	Zhuang and Matsunami, 2008	N/A
Plasmid: mouse Olfr558	Saito et al., 2009	Addgene plasmid #22333
Plasmid: human Olfr558	Saito et al., 2009	Addgene plasmid #22323
Plasmid: lentiCRISPR v2	Sanjana et al., 2014	Addgene plasmid #52961
Plasmid: $5HT_3R$	Maricq et al., 1991	N/A
Software and Algorithms		
Fastqc	Andrews, 2010	http://www.bioinformatics.babraham.ac.uk/projects/fastqc/
Scythe 0.981	Buffalo, 2011	https://github.com/ucdavis-bioinformatics/scythe
Sickle	Joshi, 2011	https://github.com/ucdavis-bioinformatics/sickle
TopHat2 v0.7	Kim et al., 2013	http://ccb.jhu.edu/software/tophat/index.shtml
Cufflinks	Trapnell et al., 2010	http://cole-trapnell-lab.github.io/cufflinks/papers/
Cuffdiff	Trapnell et al., 2013	http://cole-trapnell-lab.github.io/cufflinks/papers/
DAVID Bioinformatics Resources 6.8	Huang et al., 2009	https://david.ncifcrf.gov

METHODS

Contact for reagent and resource sharing

Further information and requests for resources and reagents should be directed to and will be fulfilled by the lead contact, David Julius (david.julius@ucsf.edu).

EXPERIMENTAL MODEL AND SUBJECT DETAILS

Animals

Mouse breeding, housing, and use was approved by the UCSF Animal Care and Use or University of Adelaide and Flinders University Animal Ethics Committees. Adult male mice of C57BL/6 background (Jackson Labs) aged 12-16 weeks with an average weight of ~29 g were used for ex vivo afferent nerve recordings and colonic sensory neuron imaging. Male mice were used in all studies to account for effects from sex or genetic background. Animals were housed in groups (2-5 mice/cage) in a specific and opportunistic pathogen free facility, fed Jackson lab diet (5K52 JL RAT & MOUSE/AUTO 6F), provided with environmental enrichment (shelter, nesting material, etc.), and had normal immune status. Reporter mice were gifts from T. Schwartz (ChgA-GFP) and M. Scanziani ($5HT_3R$-GFP).

Intestinal organoids

Adult male ChgA-GFP mice aged 6-10 weeks were used to generate intestinal organoids, as previously reported (Sato et al., 2009). Briefly, the small intestine was isolated and washed with cold PBS and crypts were isolated following dissociation in EDTA. Isolated crypts were suspended in Matrigel. Following polymerization, organoid growth media containing murine epidermal growth factor (Peprotech), noggin (Peprotech), and 10% R-spondin conditioned media was added and refreshed every 3-4 days. Organoids were maintained at 37°C, 5% CO_2 and propagated weekly. For Ca^{2+} imaging, Matrigel was removed from organoids, they were loaded with Fura-2AM, fenestrated by mechanical disturbance, and then immediately placed in the imaging chamber containing Cell-Tak (Corning)-coated coverslips. For electrophysiology, organoids were mechanically dissociated and placed on Cell-Tak coated coverslips in the recording chamber.

Cultured cells

Retrogradely traced colonic sensory neurons neurons were isolated from adult male mice following injection of cholera toxin subunit B conjugated to AlexaFluor 488 (CTB-488; Invitrogen, Carlsbad, CA) at three sites sub-serosally within the wall of the distal colon. After 4 days, lumbosacral (LS) dorsal root ganglion neurons were isolated and cultured as previously described (Brierley et al., 2009). Briefly, mice were euthanized by CO_2 inhalation and lumbosacral dorsal root ganglia (DRGs) (L6-S1) from retrogradely traced mice were surgically removed and were digested with 4 mg/mL collagenase II (GIBCO, Life Technologies) plus 4 mg/mL dispase (GIBCO) for 30 min at 37°C, followed by 4 mg/mL collagenase II for 10 min at 37°C. Neurons were then mechanically dissociated into a single-cell suspension via trituration through fire-polished Pasteur pipettes. Neurons were resuspended in DMEM (GIBCO) containing 10% FCS (Invitrogen), 2mM L-glutamine (GIBCO), 100 μM MEM non-essential amino acids (GIBCO), 100 mg/ml penicillin/streptomycin (Invitrogen) and 100ng/ml NGF (Sigma). Neurons were spot-plated on coverslips coated with poly-D-lysine (800 μg/ml) and laminin (20 μg/ml) and maintained at 37°C in 5% CO_2.

HEK293T (ATCC) were grown in DMEM, 10% fetal calf serum, and 1% penicillin/streptomycin at 37°C, 5% CO_2 and transfected using Lipofectamine 2000 (Invitrogen/Life Technologies) according to manufacturer's protocol. 1 μg of human Adrα2A or TRPC4β was transfected for independent expression with 0.2 μg GFP. For coexpression experiments, equal concentrations of Adrα2A and TRPC1, TRPC3, TRPC4, or TRPC6 were used. Constitutively active (Q205L) or dominant-negative (G203T) $G\alpha_{i2}$ mutants were included in the transfection mix for some experiments. For Olfr558 experiments, 1.5 μg of Olfr558 was transfected with several constructs used enhance expression and signaling of olfactory receptors in heterologous systems: 1 μg of receptor-transporting protein 1 short (RTP1S), guanine nucleotide exchange factor B (Ric8b), and $G\alpha_{olf/15}$, and 0.2 μg GFP for cellular identification. Mock transfection experiments were performed by transducing all constructs except Olfr558. Human Adrα2A was from Genscript (Piscataway, NJ), $G\alpha_{i2}$ mutants from cDNA Resource Center; TRPC1, TRPC3, and TRPC6 were cloned into pcDNA3 in the Julius lab; TRPC4 was a gift from J. Jeon and M. Zhu; Olfr558 constructs were gifts from H. Matsunami (Addgene) and were tagged with the first 20 residues of human rhodopsin to increase expression; RTP1S, Ric8b, and $G\alpha_{olf/15}$ were gifts from A. Chang. lentiCRISPR v2 was a gift from F. Zhang (Addgene).

METHOD DETAILS

CRISPR-mediated gene disruption

gRNA sequences were designed with the Cas9 design target tool (http://crispr.mit.edu) and inserted into the Cas9-containing lentiCRISPR v2 vector (Sanjana et al., 2014). Primers used to design the specific gRNA target were: Olfr558 forward (5′ to 3′) CACCGagcacagtggcatgccgtag; Olfr558 reverse (5′ to 3′) AAACctacggcatgccactgtgctC. Lentivirus was produced by transfecting HEK293T cells with psPAX2, pVSVG and LentiCRISPR v2 with Olfr558 gRNA using Fugene HD (Roche) according to the manufacturer's instructions. Virus was concentrated and re-suspended in organoid growth medium. As a control for both sequencing and functional experiments, organoids were infected with empty Cas9-containing LentiCRISPR v2 vector. Vector-infected organoids expressed wild-type Olfr558 sequence and exhibited similar isovalerate-induced Ca^{2+} responses compared with wild-type organoids, so were grouped with other controls in some analyses.

Two days before infection, intestinal organoids were grown in a 24-well culture plate with growth medium supplemented with 5 μM CHIR99021 (Sigma) and 10 mM nicotinamide (Sigma) to increase stem cell population. Stem cell-enriched organoids were broken down into single-cells, viral mix was added, and cells were transferred to a 48-well plate that was centrifuged at 600 g for 60 min (spinoculation) and placed in the incubator for another 6 hr at 37°C. Cells were collected, re-suspended in Matrigel, and transferred into a 24-well culture plate. After two days of recovery, selection was carried out using puromycin (6 μg/ml) for three days. After selection, growth medium was supplemented with 5 μM CHIR99021 and 10 mM nicotinamide. Organoids were then treated with TrypLE (Life Technologies) at 37°C for 5 min to achieve single cells which were plated onto 96-well culture plates for clonal selection. Growth medium was supplemented with 5 μM CHIR99021, 10 μM Y-27632 (Sigma) and 10 mM nicotinamide during the first two days after plating to enrich for stem cells and prevent apoptosis. The medium was then changed to growth medium supplemented with 5 μM CHIR99021 and 10 mM nicotinamide for another three days and then normal growth medium afterward. Single organoids were then collected and used for clonal expansion. To verify clonal populations genetic disruption, genomic DNA was isolated using QuickExtract DNA extraction solution (Epicenter) and PCR amplified using Phusion polymerase (NEB) and the following primers for Olfr558: F: ctttgcatgctttctggcct; R: tgcaggtgttcttccattcca. Products were cloned into Topo vectors (Agilent) and sequenced.

Electrophysiology

Recordings were carried out at room temperature using a MultiClamp 700B amplifier (Axon Instruments) and digitized using a Digidata 1322A (Axon Instruments) interface and pClamp software (Axon Instruments). Data were filtered at 1 kHz and sampled at 10 kHz and leak-subtracted online using a P/4 protocol for voltage step protocols. Membrane potentials were corrected for liquid junction potentials. EC cells were identified by GFP expression and recordings were made using borosilicate glass pipettes polished to 7 - 9 MΩ. Recording pipettes used for HEK293 were 3 - 4MΩ. Unless stated otherwise, a standard Ringer's extracellular solution for EC and HEK293 cell experiments contained (mM): 140 NaCl, 5 KCl, 2 $CaCl_2$, 2 $MgCl_2$, 10 HEPES, 10 glucose, pH 7.4. Intracellular solution for recording K^+ currents from EC cells contained: 140 K-gluc, 5 KCl, 1 $MgCl_2$, 10 K-EGTA, 10 HEPES, 10 sucrose, pH 7.2. Intracellular solution for current-clamp recordings contained: 140 K-gluc, 5 NaCl, 1 $MgCl_2$, 0.02 K-EGTA, 10 HEPES,

10 sucrose, pH 7.2. Other EC cell and $5HT_3R$ recordings used the following intracellular solution: 140 $CsMeSO_4$, 5 NaCl, 1 MgCl2, 10 Cs-EGTA, 10 HEPES, 10 sucrose, pH 7.2. Intracellular solution for Adrα2A-expressing cells contained 0.1 Cs-EGTA. For EC recordings, holding potential was −90 mV and currents were elicited by 500ms ramps from −100 mV to +100 mV or 200ms steps in 10 mV increments. G-V relationships were derived from I-V curves by calculating G: $G = I_{Ca} / (V_m - E_{rev})$ and were then fit with a Boltzman equation. Voltage-dependent inactivation was measured during −10 mV voltage pulses following a series of 1 s prepulses ranging from −110 to 60 mV in 10 mV increments. Voltage-dependent inactivation was quantified as I / I_{max}, with I_{max} occurring at the voltage pulse following a −110 mV prepulse. Adrα2A-associated experiments were carried out using a protocol that consisted of 10 s holding voltage at −60mV followed by a 500 ms ramp from −100 mV to +100 mV that returned to −60 for an additional 10 s, and this protocol was repeated consecutively for ~10 min or more. For $5HT_3R$ biosensor recordings, whole-cell configuration was achieved and cells were lifted from coverslips and moved immediately adjacent to GFP-labeled EC cells. Voltage has held constant at −80 mV as solutions were washed on and off with local perfusion. Responses were normalized to peak current induced by mCPBG.

Calcium imaging

EC and HEK were loaded with 10 μM Fura-2-AM (Invitrogen) and 0.01% Pluronic F-127 (wt/vol, Invitrogen) for 1 h in Ringer's solution. 340 nm to 380 nm ratio was acquired using MetaFluor software. EC cells were identified by GFP expression and responses were normalized to increased fluorescence ratio elicited by high extracellular K^+ (K^+, 140 mM) at the end of the experiment. In most experiments, only one EC cell was identified in the field of view, thus we quantified data from single cells. In somewhat rare cases when two EC cells were observed in the same field of view, responses were averaged. Dorsal root ganglion neurons were cultured for 24 hr, incubated with 2.5 μM Fura2-AM and 0.02% (v/v) pluronic acid for 30 min at room temperature in modified Ringer's solution containing (mM): 145 NaCl, 5 KCl, 1.25 $CaCl_2$, 1 $MgCl_2$, 10 glucose, 10 HEPES. After a brief wash, coverslips were transferred to the recording chamber and Ca^{2+} responses were measured at room temperature. Colonic DRG neurons were identified by the presence of the 488 tracer and viability was verified by responses to 25 mM KCl. All pharmacological agents were delivered by local perfusion with exception of 1 μM U73122, 100 μM gallein, 200 ng/ml cholera toxin, or 200 ng/ml pertussis toxin, 10 μM SQ22536, which were preincubated. Associated vehicle control experiments were performed. In experiments using HEK293, construct-expressing cells identified by GFP expression were quantified and responses were normalized to maximal responses elicited by 1 μM ionomycin at the end of the experiment.

Concentrations and abbreviations of molecules used in Ca^{2+} imaging screening (in μM): 1 Capsaicin, 500 allyl isothiocyanate (AITC), 50 1-(m-chlorophenyl)-biguanide (mCPBG), 1 icilin, 200 N-butyryl-L-Homoserine lactone (C4-HSL), 200 N-hexanoyl-L-Homoserine lactone (C6-HSL), 200 N-3-oxo-dodecanoyl-L-Homoserine lactone (3OC12-HSL), 1 or 10 *N*-Formylmethionine-leucyl-phenylalanine (fMFL), 50 μg/ml lipopolysaccharide (LPS) from E. Coli, 500 indole, 500 sodium propionate, 500 sodium acetate, 500 sodium butyrate, 500 isobutyrate, 500 isovalerate, 500 sodium deoxycholate, 1 substance P, 100 histamine, 1000 glutamate, 100 tryptamine, 100 serotonin, 100 glycine, 100 gamma-aminobutyric acid (GABA), 100 dopamine, 100 epinephrine, 100 norepinephrine. Unless stated otherwise, concentrations of other pharmacological agents (in μM): 0.5 tetrodotoxin (TTX), 10 nifedipine, 0.3 ω-agatoxin IVA, 0.3 ω-conotoxin, 5 mibefradil, 1 epinephrine, 1 norepinephrine, 5 yohimbine, 10 isoproterenol, 5 prazosin, 5 clonidine, 5 propranolol, 10 phenylephrine, 5 U73122, 100 gallein, 200ng/ml pertussis toxin (PTX), 200ng/ml cholera toxin (CTX), 50 2-aminoethoxydiphenyl borate (2-APB), 10 ML204. Most drugs were from Tocris, HSLs and 4-hydroxynonenal were from Cayman Chemical, volatile fatty acids were from Sigma.

Transcriptome sequencing and analysis

Intestinal epithelial cells from organoids were dissociated and immediately sorted by fluorescence-activated cell sorting (FACS) by the Laboratory for Cell Analysis at UCSF. ~1% of total epithelial cells were GFP^+ and collected. The remaining GFP^- cells were retained for comparison. RNA from GFP^+ and GFP^- subgroups was then extracted and prepared for cDNA library generations using the SMARTer Ultra Low Input RNA kit followed by the Low Input Library Prep Kit (version 2, Clontech Laboratories, Inc.). cDNA quality was assessed via bioanalyzer using the High Sensitivity DNA kit (Agilent Technologies), and high quality samples were preserved for sequencing.

PolyA cDNA libraries were sequenced on the Illumina Hi-Seq 4000 platform (QB3 Vincent J. Coates Genomic Sequencing Library), generating 150 bp paired-end reads. More than 100M reads were obtained. The quality of raw sequence reads was analyzed via FASTQC. Adapters were trimmed using Scythe, and sequence read ends were trimmed using Sickle. Reads were then aligned to the annotated mouse reference genome (mm10) using TopHat2 (version 0.7). Transcripts were assembled and relative abundance was estimated using Cufflinks and Cuffdiff tools. Gene ontology-based (GO) analyses were carried out using DAVID (version 6.8) to categorize the top ~1000 transcripts annotated with ENSEMBL gene IDs that showed the greatest fold change between GFP^+ and GFP^- samples. The "biological process" set of GO terms was used in functional annotation of the enriched transcripts in the GFP^+ sample over the GFP^- sample, which was set as the background.

Histology

Immunofluorescence (IF) was performed using 5 μm cryosections. Blocking was performed with 10% normal serum corresponding to secondary antibody species in 0.1% Triton-X and PBS at room temperature for 60 min. Primary antibodies were incubated overnight at 4°C at the indicated dilutions. Antibodies used were against ChgA (1:200, Santa Cruz), serotonin (1:10,000, Immunostar), Adrα2A (1:200, Affinity Bioreagents), tyrosine hydroxylase (1:500, Millipore), Synapsin (1:500, from R. Edwards), PSD-95 (1:200,

Neuromab), Lysozyme (1:200, Dako), GLP-1 (1:200, Abcam), Substance P (1:1000, Penninsula). Alexa Fluor-conjugated secondary antibodies were used at 1:300-1000 (Millipore). In situ hybridization histochemistry was performed using digoxigenin- and fluorescein-labeled cRNA for mouse TRPC4 or Olfr558. Probes were generated by T7/T3 in vitro transcription reactions using a 500-nucleotide fragment of TRPC4 (nucleotides 1553 to 2053), and a 500-nucleotide fragment of Olfr558 cDNA (nucleotides 1000 to 1500). Hybridization was developed using anti-digoxigenin and anti-fluorescein Fab fragments, followed by incubation with FastRed and streptavidin-conjugated Dylight 488 according to published methods (Ishii et al., 2004). Epifluorescence imaging was performed on an Olympus IX51 microscope equipped with a DP71 imager and Nikon Eclipse Ti with a DS-Qi2 imager. Confocal imaging was performed on Nikon Ti microscope with Yokogawa CSU-22 spinning disk. Images were assembled in Photoshop and ImageJ. Surface rendering was performed using UCSF Chimera.

Single nerve fiber recordings of pelvic colonic mucosal afferents

C57BL/6J male mice were humanely euthanized by CO_2 inhalation. The colon and rectum with attached pelvic nerves were removed and recordings from mucosa afferents were performed as previously described (Brierley et al., 2004). Briefly, the colon was removed and pinned flat, mucosal side up, in a specialized organ bath. The colonic compartment was superfused with a modified Krebs solution (in mM: 117.9 NaCl, 4.7 KCl, 25 $NaHCO_3$, 1.3 NaH2PO_4, 1.2 MgSO4, 2.5 $CaCl_2$, 11.1 D-glucose), bubbled with carbogen (95% O_2, 5% CO_2) at a temperature of 34°C. All preparations contained the L-type calcium channel antagonist nifedipine (1 μM) to suppress smooth muscle activity and the prostaglandin synthesis inhibitor indomethacin (3 μM) to suppress potential inhibitory actions of endogenous prostaglandins. The pelvic nerve bundle was extended into a paraffin-filled recording compartment in which finely dissected strands were laid onto a mirror, and a single fiber placed on the platinum recording electrode. Action potentials recorded in response to mechanical or chemical stimuli were discriminated as single units based on Waveform, amplitude and duration using spike software (Cambridge Electronic Design, Cambridge, UK).

Colonic afferents were classified by identifying receptive fields by systematically stroking the mucosal surface with a still brush to activate all subtypes of mechanoreceptors. Categorization of afferents properties was in accordance with our previously published classification system (Brierley et al., 2004). In short, pelvic mucosal afferents respond to fine mucosal stroking (10 mg von Frey hairs; vfh), but not to circular stretch. Stimulus–response functions were constructed by assessing the total number of action potentials generated in response to mechanical stimuli (mucosal stroking with 10, 200, 500 and 1000 mg vfh). Norepinephrine (NE, 1 μM) was applied for 15 min via a small metal ring placed over the receptive field of interest and the TRPC4 inhibitor ML204 (10 μM) or the 5-HT_3R antagonist alosetron (10 μM) were pre-incubated for 10 min prior, and co-applied with NE. This route of administration has been previously shown to reproducibly activate afferent fibers (Brierley et al., 2009).

QUANTIFICATION AND STATISTICAL ANALYSIS

Data were analyzed with Clampfit (Axon Instruments) or Prism (Graphpad) and are represented as mean ± sem and n represents the number of cells or independent experiments. Data were considered significant if $p < 0.05$ using paired or unpaired two-tailed Student's t tests or one- or two-way ANOVAs. Statistical parameters are described in figure legends. All significance tests were justified considering the experimental design and we assumed normal distribution and variance, as is common for similar experiments. Sample sizes were chosen based on the number of independent experiments required for statistical significance and technical feasibility.

DATA AVAILABILITY

The accession number for the deep sequencing data reported in this paper is GEO: GSE98794. All other data are available from the authors upon request.

Cell

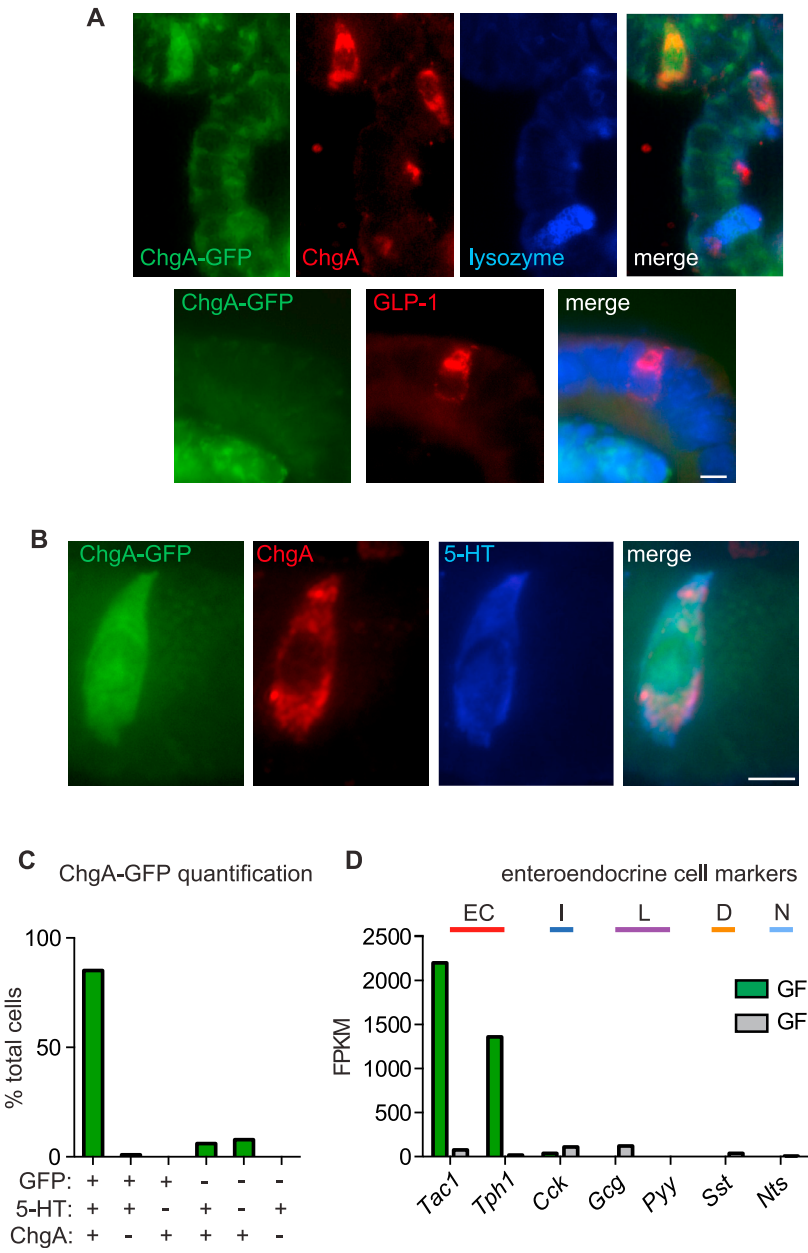

Figure S1. ChgA-GFP Is a Marker for Enterochromaffin Cells, Related to Figure 1

(A) Chromogranin A-GFP (ChgA-GFP, green) did not colocalize with lysozyme (top, blue) or GLP-1 (bottom, red). Scale bar: 10 μm.

(B) ChgA-GFP (green) colocalized well with ChgA (red) and serotonin (5-HT, blue). Scale bar: 10 μm.

(C) In intestinal organoids, the majority of ChgA-GFP-expressing cells colocalized with 5-HT and ChgA (97/114). Importantly, we did not observe any GFP-expressing cells that were negative for 5-HT. ChgA-GFP signal was relatively dim and some signal was lost in tissue processing and quantification, likely contributing to a minority of GFP-negative cells that expressed ChgA and 5HT (7/114) or ChgA (9/114).

(D) mRNA expression profile of various enteroendocrine cell type markers (I, L, D, N, S cells) in ChgA-GFP^{+} cells demonstrates that ChgA-GFP primarily labels enterochromaffin (EC) cells. Bars represent fragments per kilobase of exon per million fragments mapped (FPKM).

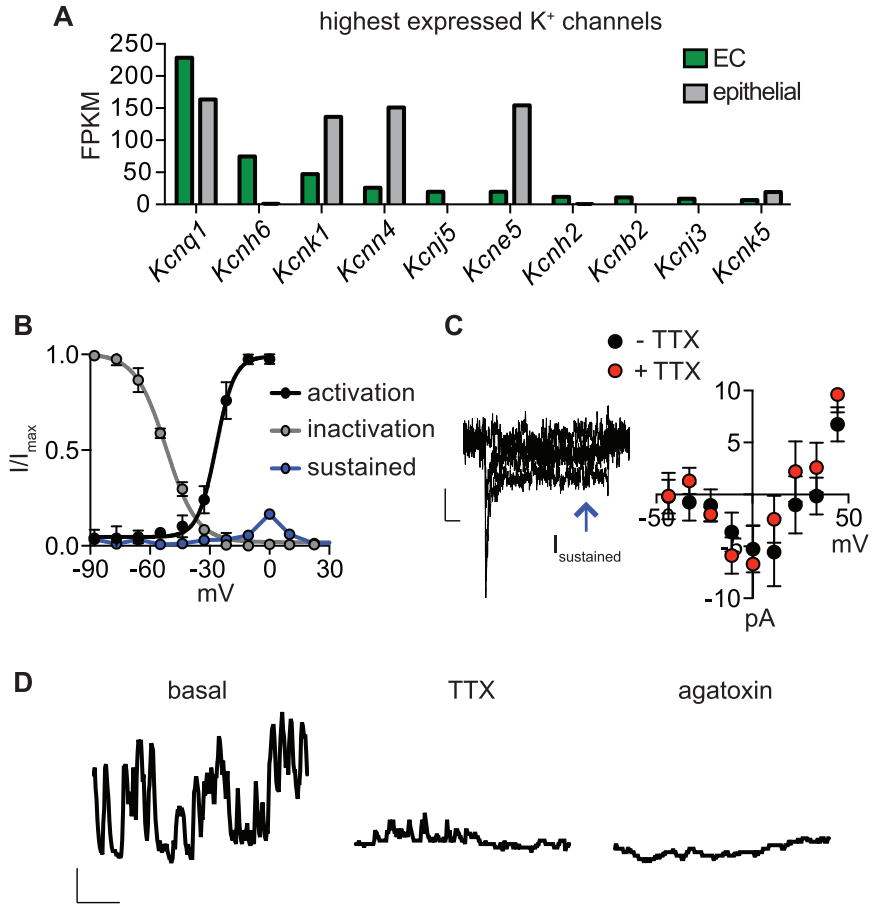

Figure S2. Voltage-Gated Ion Channels in Enterochromaffin Cells, Related to Figure 1

(A) 10 Highest expressed K^+ channel transcripts in EC cells. Bars represent fragments per kilobase of exon per million fragments mapped (FPKM).

(B) G-V relationship of transient Na_V current reveals half-maximal activation voltage ($V_{a1/2}$) of −26.8 ± 1.2 mV (black). Inactivation-voltage relationship had half-inactivation potential ($V_{h1/2}$) of −52 ± 0.8 mV (gray). Small amplitude, sustained, TTX-insensitive, voltage-gated current measured at the end of voltage pulses is represented in blue. n = 6.

(C) Representative slowly-inactivating, tetrodotoxin (TTX, 500nM)-insensitive, voltage-gated currents. Scale bar: 10pA, 25ms. Average current-voltage relationship in the presence or absence of TTX. n = 4 cells. All data represented as mean ± sem.

(D) Representative basal Ca^{2+} bursting activity observed in a small subset of EC cells. This "bursting" activity in EC cells was reduced by tetrodotoxin (TTX, 500 nM) and abolished by ω-agatoxin IVA (300 nM). Scale bar: 0.1 Fura-2 ratio, 100 s. Representative of n = 3.

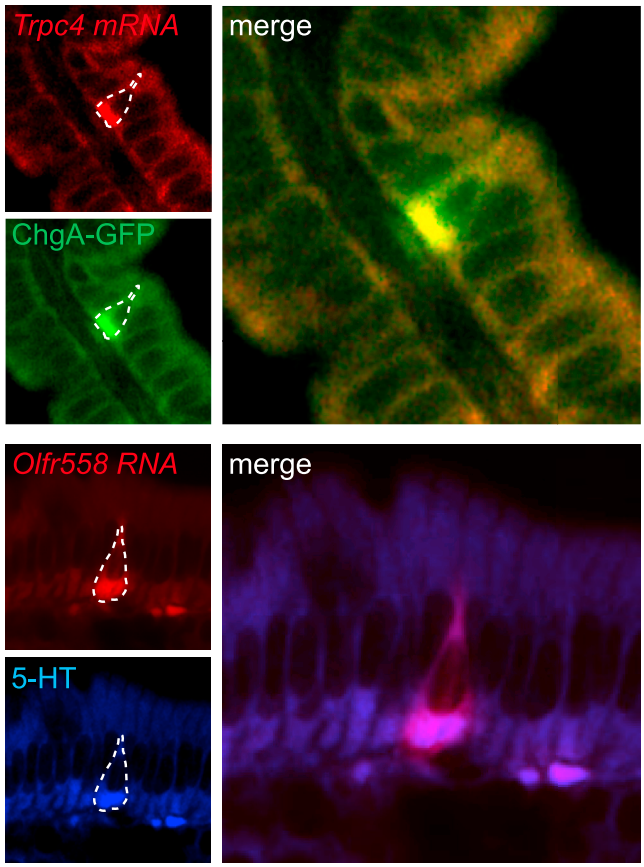

Figure S3. Sensory Receptor/Transducer Expression in Native Enterochromaffin Cells, Related to Figure 2

Trpc4 (red, *top panels*) and *Olfr558* (false-colored red, *bottom panels*) transcripts co-localized with native EC cells marked by ChgA-GFP (green, *top*) or serotonin (5-HT, blue, *bottom*). Merged images are shown for each probe (*right*).

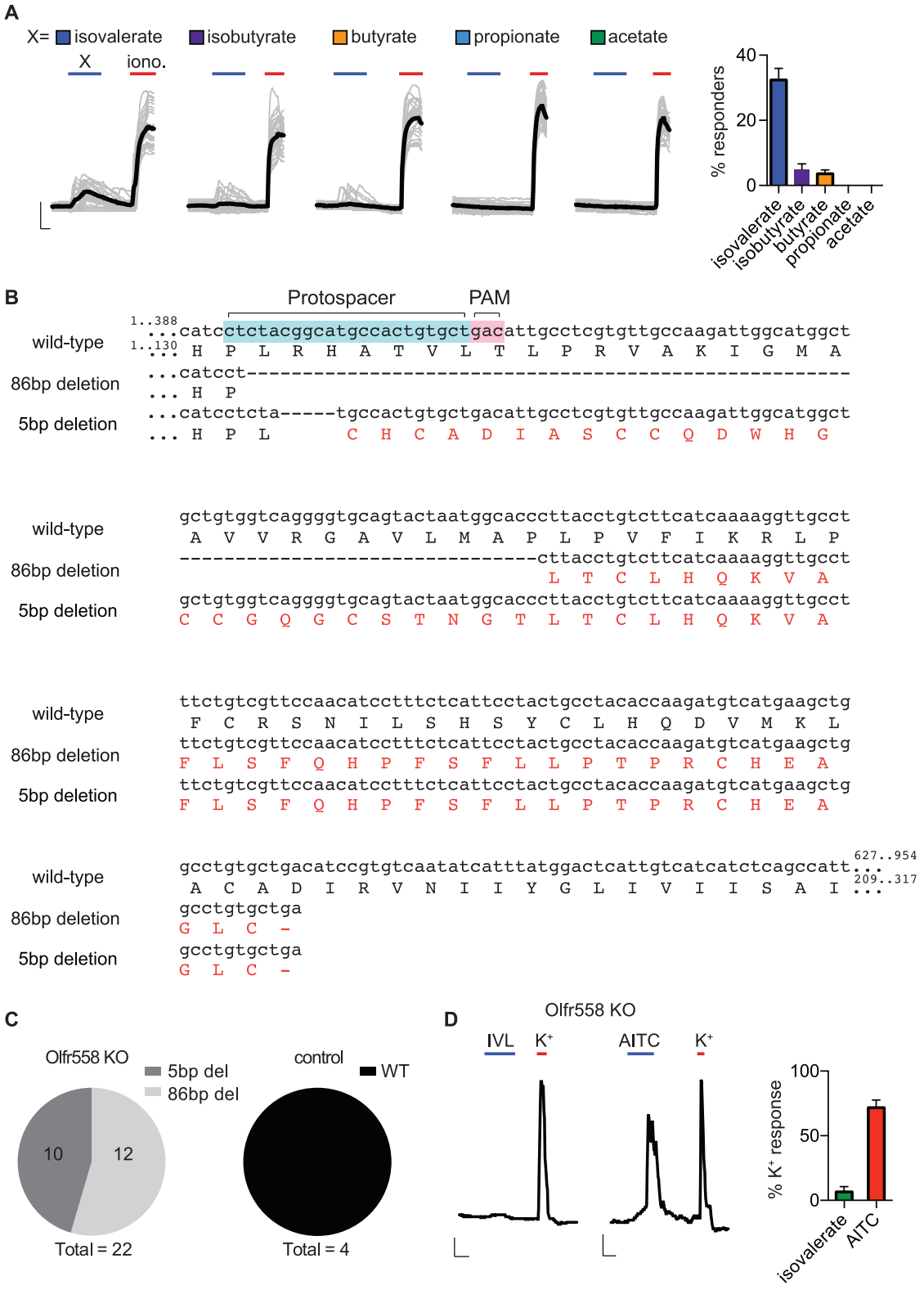

Figure S4. Targeted Disruption of Olfr558 in ChgA-GFP Intestinal Organoids Using CRISPR, Related to Figure 2

(A) Metabolite-induced Ca^{2+} responses from HEK293 cells expressing human Olfr558 with the $G\alpha_{olf/15}$ chimera to facilitate coupling of Olfr558 to Ca^{2+} release. The largest percentage of cells responded to 100 μM isovalerate. Fewer cells responded to isobutyrate (100 μM) or butyrate (100 μM) and equal concentrations of

(legend continued on next page)

propionate or acetate did not induce activity. Ionomycin (iono, 1 μM) was added at the end of each experiment to induce maximal Ca^{2+} responses. Black traces represent an average of all cells in the field shown in gray. Scale bar: 0.2 Fura-2 ratio, 50 s. Average percentage of responding cells was calculated by quantifying all ionomycin-responsive cells expressing GFP. n = 5 per condition. Data represented as mean ± sem.

(B) Sequencing from Olfr558 knockout (KO) organoids. ChgA-GFP intestinal organoids were generated from single stem cells infected with a lentiviral CRISPR/Cas9 construct targeting Olfr558. Two mutations were detected in KO organoids and both deletions resulted in an early stop codon. Numbers indicate base pair or amino acid positions.

(C) Frequency of deletions or wild-type sequences observed in organoids infected with CRISPR/Cas9 to target Olfr558 compared with organoids infected with Cas9-containing vector as a control.

(D) AITC (150 μM), but not isovalerate (IVL, 200 μM), evoked large Ca^{2+} responses in Olfr558 knockout (KO) ChgA-GFP organoids generated using CRISPR. Scale bar: 0.1 Fura-2 ratio, 50 s.

(E) Average AITC-elicited Ca^{2+} responses in Olfr558 KO organoids. Averaged isovalerate data from Figure 2 shown for comparison. n = 3 for AITC and n = 6 for isovalerate.

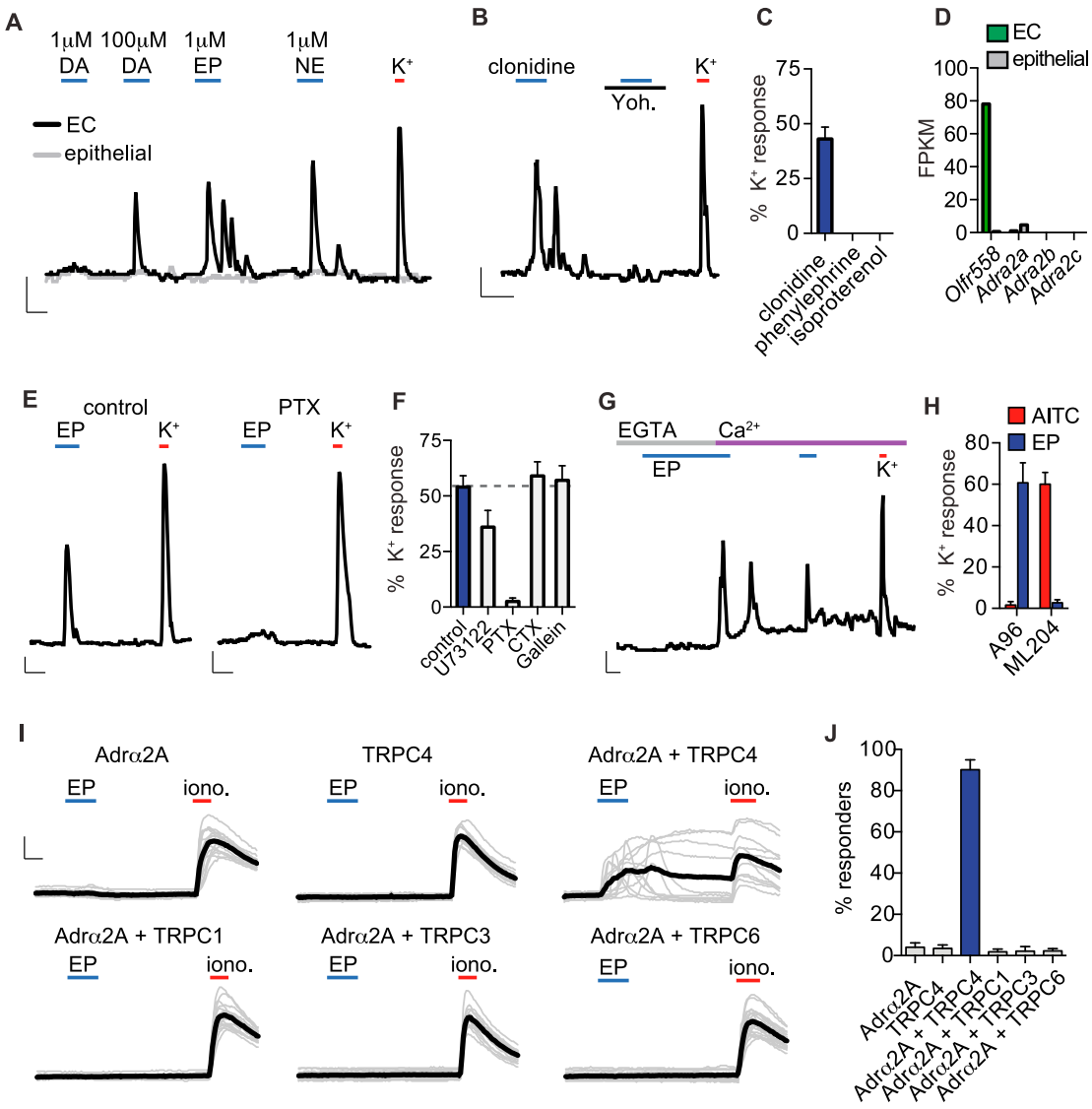

Figure S5. Adrα2A and TRPC4 Mediate Catecholamine Signal Transduction, Related to Figure 3

(A) Representative catecholamine responses in EC cells (black) or neighboring epithelial cells (gray). High concentrations of dopamine (DA, 100 μM) were required to elicit responses similar to lower concentrations of epinephrine (EP, 1 μM) or norepinephrine (NE, 1 μM). Scale bar: 0.1 Fura-2 ratio, 50 s.

(B) Representative Ca^{2+} traces demonstrating that the Adrα2 agonist clonidine (5 μM) elicits responses that are inhibited by yohimbine (yoh, 5 μM). Scale bar: 0.1 Fura-2 ratio, 50 s.

(C) Pharmacological profile of adrenoreceptor agonists. n = 5 per condition.

(D) mRNA expression profile of α-adrenoreceptors in EC cells versus other intestinal epithelial cells. The EC cell-enriched GPCR Olfr558 is shown for comparison. Bars represent fragments per kilobase of exon per million fragments mapped (FPKM).

(E) Representative epinephrine (EP, 1 μM) responses were blocked by pertussis toxin (PTX, 200ng/ml). Scale bar: 0.1 Fura-2 ratio, 50 s.

(F) Pharmacological profile of epinephrine-evoked Ca^{2+} responses. n = 5 per condition. $p < 0.0001$ for control versus PTX. One-way ANOVA with post hoc Bonferroni test.

(G) Representative trace demonstrating that EP responses were absent in Ca^{2+} free extracellular solution, but were consistently evoked in the presence of Ca^{2+}. Scale bar: 0.1 Fura-2 ratio, 50 s.

(H) EP-evoked responses were blocked by the TRPC4 inhibitor ML204 (10 μM), but not the TRPA1 inhibitor A967079 (A96, 10 μM). AITC (150 μM)-evoked responses were blocked by A967079, but not ML204. n = 4 per condition. $p < 0.0001$, two-way ANOVA with post hoc Bonferroni test.

(I) EP (1 μM) did not elicit Ca^{2+} responses HEK293 independently expressing Adrα2A or TRPC4, but evoked large responses in cells cotransfected with Adrα2A and TRPC4. EP did not elicit responses in cells cotransfected with Adrα2A and TRPC1, TRPC3, or TRPC6. Ionomycin (iono, 1 μM) was added at the end of each experiment to induce maximal Ca^{2+} responses used for normalization. Black traces represent an average of all cells in the field shown in gray. Scale bar: 0.2 Fura-2 ratio, 25 s.

(J) Average Ca^{2+} responses normalized to iono. n = 6 experiments per condition. All data represented as mean ± sem. $p < 0.0001$, one-way ANOVA with post hoc Bonferroni test.

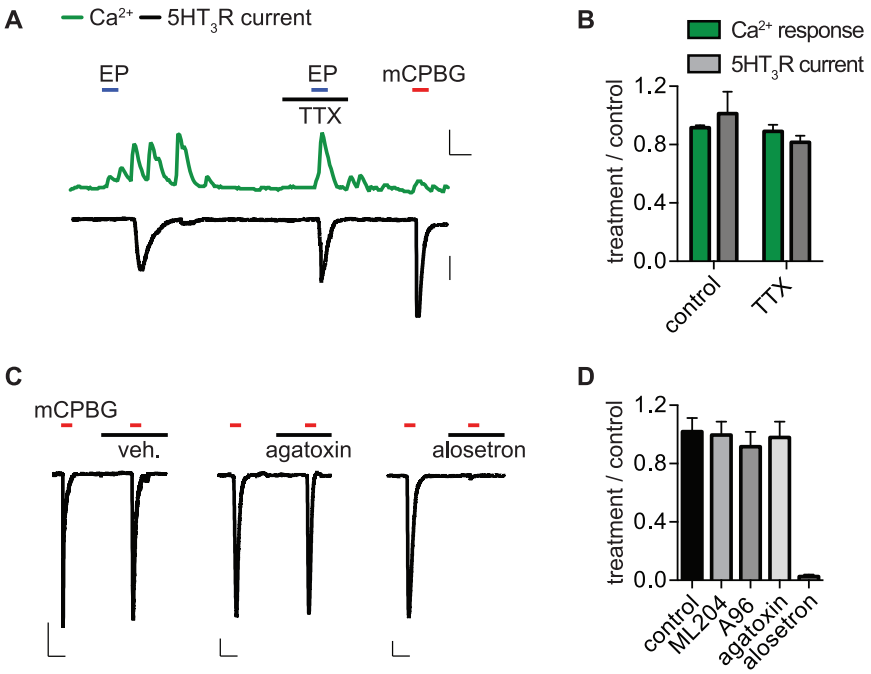

Figure S6. 5-HT Biosensor Controls, Related to Figure 4

(A) Representative EP-evoked Ca^{2+} responses (green) and $5HT_3R$ currents (black) were not affected by TTX (500nM). 0.3 Fura-2 ratio, 50 s, 500pA.

(B) Average peak EC Ca^{2+} responses and associated $5HT_3R$-expressing HEK293 currents. n = 4 per condition. Data represented as mean ± sem.

(C) Representative currents evoked by mCPBG (5 μM) in $5HT_3R$-expressing HEK293 cells were not affected by ω-agatoxin IVA (300nM), but were blocked by the $5HT_3R$ antagonist alosetron (200nM). Scale bars: 200pA, 60 s.

(D) Averaged normalized maximal $5HT_3R$ currents were inhibited by alosetron (200nM), but were not significantly affected by ML204 (10 μM), A967079 (A96, 10 μM), or ω-agatoxin IVA (300nM). Data represented as mean ± sem. n = 3 per condition. $p < 0.0001$, one-way ANOVA with post hoc Bonferroni test.

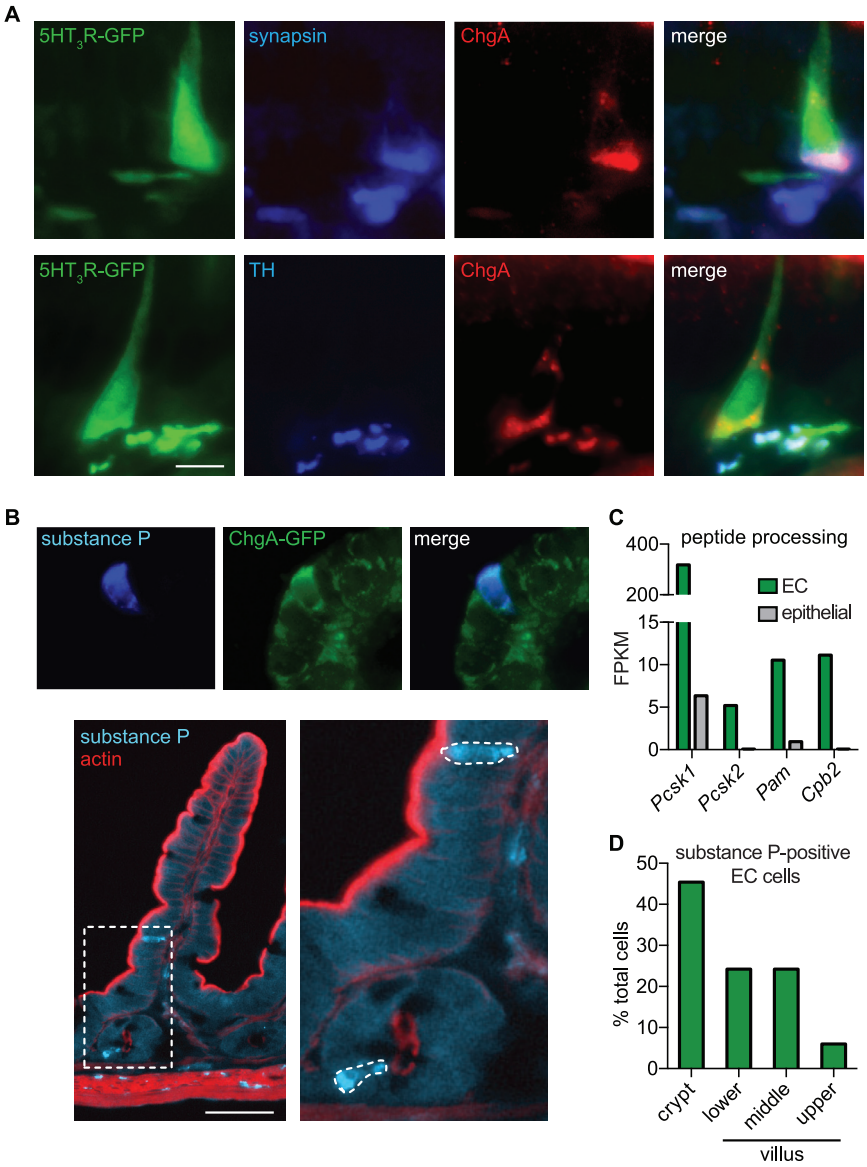

Figure S7. Intestinal Expression of Neural Markers and Signaling Molecules, Related to Figure 5

(A) $5HT_3R$-GFP fibers on the basolateral side of epithelium colocalized with synapsin, indicating their expression in nerve fibers. $5HT_3R$-GFP was also expressed in subsets of intestinal epithelial cells, including some ChgA-positive cells, but we did not observe mCPBG-evoked responses in epithelial cells or $5HT_3R$ expression in our RNA-seq dataset. This observation is consistent with previous studies demonstrating that $5HT_3R$ is transiently expressed in certain tissues during development (Tecott et al., 1995). Scale bar: 10 μm. Tyrosine hydroxylase (TH) was expressed in fibers near epithelial cells and sometimes colocalized with $5HT_3R$-GFP. Scale bar: 10 μm.

(B) Substance P (blue) was expressed in EC cells (ChgA-GFP, green). Scale bar: 10 μm. Substance P (blue) expression in EC cells was most prominent in crypts and decreased as cells were localized toward villus tips. Actin staining (red) demonstrates intestinal architecture. Scale bar: 50 μm.

(C) Anatomical distribution of substance P-expressing EC cells. 33 total cells counted.

(D) Peptide processing transcripts are enriched in EC cells (green) compared with other intestinal epithelial cells (gray). *Pcsk1* = proprotein convertase/kexin type 1; *pcsk2* = proprotein convertase/kexin type 2; *pam* = peptidylglycine alpha-amidating monooxygenase; *cpb2* = carboxypeptidase B2. Bars represent fragments per kilobase of exon per million fragments mapped (FPKM).

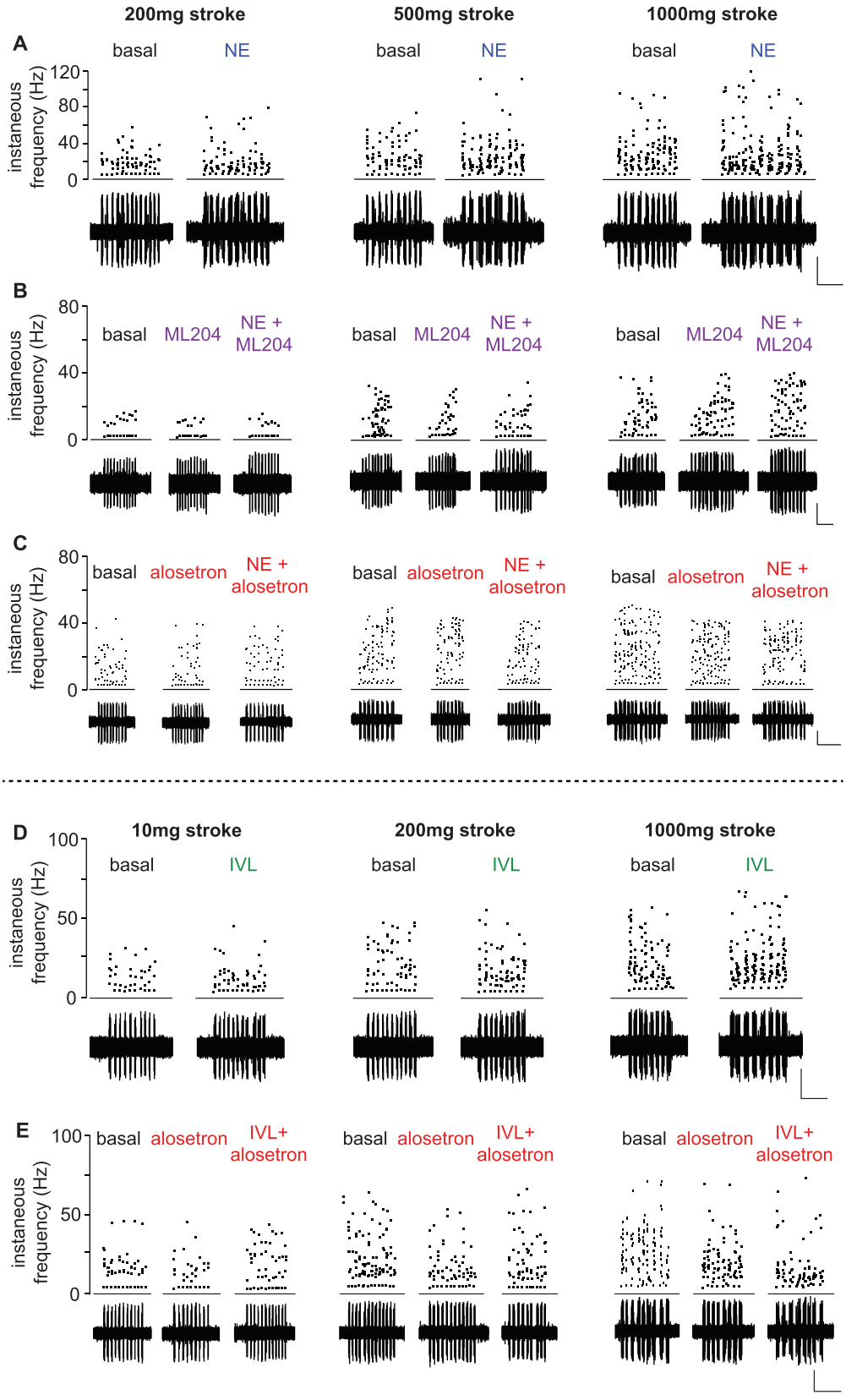

(legend on next page)

Figure S8. Epithelial Norepinephrine or Isovalerate Modulates Mechanosensitivity of Colonic Afferent Nerve Fibers, Related to Figure 7

(A–C) Representative mechanical responses recorded from single mucosal colonic afferent nerve fibers. Norepinephrine (NE, 1 μM) enhanced responses elicited by 200mg, 500mg, 1000mg von Frey hair mucosal stroking. Norepinephrine-induced mechanical hypersensitivity was blocked by ML204 (10 μM) or alosetron (10 μM). Scale bars: NE = 400 μV, 10 s, NE+ML204 = 500 μV, 10 s, NE+alosetron = 500 μV, 10 s.

(D and E) Representative mechanical responses recorded from single mucosal colonic afferent nerve fibers. Isovalerate (IVL, 200 μM) enhanced responses elicited by 10mg, 200mg, 1000mg von Frey hair mucosal stroking. Isovalerate-induced mechanical hypersensitivity was blocked by alosetron (10 μM). Scale bars: 500 μV, 10 s.